SHOCK-WAVE STRUCTURE IN A SINGLE COMPONENT MONATOMIC GAS

MURAOKA, Katsunori
Research Institute for Applied Mechanics, Kyushu University : Research Associate

https://doi.org/10.5109/7170829

出版情報：Reports of Research Institute for Applied Mechanics. 16 (54), pp.295-333, 1968. 九州大学応用力学研究所
バージョン：
権利関係：

Reports of Research Institute for Applied Mechanics
Vol. XVI, No. 54, 1968

SHOCK-WAVE STRUCTURE IN A SINGLE COMPONENT MONATOMIC GAS

By

Katsunori MURAOKA*

The one-dimensional, steady, neutral shock wave structure was theoretically investigated by expanding the distribution function of the Boltzmann equation in terms of the Hermite polynomial, where the downstream equilibrium distribution function is taken to be the weighting function. The resulting non-linear coupled differential equations are numerically integrated and various thermodynamic variables are calculated. Then the reasonable results are obtained for low (where Navier-Stokes approximation is thought to be correct) and high (where Mott-Smith treatment is seen to be appropriate) Mach numbers. The thermodynamic backgrounds of the present treatment have thoroughly discussed and the criticisms to the various other theoretical methods have been done.

I. Introduction

Energy dissipation mechanisms play the dominant roles in the problem of the shock wave structure in gases, so much as in the case of the boundary layer. While the complex interactions of the gas phase with the solid surface make it difficult for the boundary condition to be taken into the formulations for the problem of boundary layer, the boundary conditions are very clear for the shock structure problem as they can be specified as the thermodynamic equilibrium states at the up- and down-stream infinity points of the shock wave. Further, the Navier-Stokes equations, formulated on the ground of linear dissipations, would give fairly good descriptions of the phenomena for the boundary layer, but we must resort to the kinetic theory to express the shock structure problem, as the temperature and velocity gradients may become very steep, especially so at high Mach numbers, and it would become insufficient for us to assume the linear dissipations.

Many theoretical investigations[1)~4)] have been made for the one-dimensional, steady shock structure, and at the same time, experimental studies, centering mainly on measuring the density profiles across the shock front, have been performed using various techniques[5)~11)]. As the results, the following is believed to be true for the monatonic gas shock structure without the excitation of the internal degrees of freedom; i.e., for low Mach numbers ($1 \leq M \leq 1.5$) the Navier-Stokes formulation[2)] gives fair description, while the Mott-Smith bimodal distribution function method[3)] expresses the phenomena

* Research Associate, Research Institute for Applied Mechanics, Kyushu University.

properly for higher Mach numbers ($M \geq 2.0$). Furthermore, the bimodal distribution function of Mott-Smith cannot be expressed by the Navier-Stokes approximation and vice versa[12]. Then, the author proposes a more reasonable assumption to the distribution function than that of Mott-Smith and tries to express well the state within the shock wave in the whole range of Mach numbers covered by the above two theories.

The kinetic states of the perfect gas are expressed, from the upstream, in the shock wave, to the downstream, by the Boltzmann equation which will be written for the problem of the one-dimensional, steady state as follows[13];

$$u\frac{\partial f}{\partial x}=\iiint (f_1'f'-f_1f)\,gbdbd\varepsilon d\mathbf{c}_1 \quad , \tag{1}$$

where $f(\mathbf{r}, \mathbf{c}, t)$ denotes the distribution function, $\mathbf{r}$ the space coordinate (the orthogonal three components are denoted by x, y and z), $\mathbf{c}$ the velocity (u, v and w will represent the x, y and z component of $\mathbf{c}$, respectively), g the relative velocity, b the impact parameter, and ε the azimuth angle. The right-hand side of Eq. (1) expresses the change of f due to the collisions where the primed quantities represent the values after the collisions. Here, the y-z plane is taken on that of the shock wave and the x axis perpendicular to it. And we adopt the shock coordinate (i. e., the shock wave is fixed in the space), the flow being from $x=-\infty$ to $x=\infty$.

It is difficult to exactly solve thisBoltzmann integro-differential equation under the given boundary conditions, which are

$$\left.\begin{aligned} f=n_uf_u&=n_u\left(\frac{1}{2\pi RT_u}\right)^{3/2} exp\left\{-\frac{(\mathbf{c}-\mathbf{i}u_u)^2}{2RT_u}\right\} \quad \text{at } x=-\infty,\\ f=n_df_d&=n_d\left(\frac{1}{2\pi RT_d}\right)^{3/2} exp\left\{-\frac{(\mathbf{c}-\mathbf{i}u_d)^2}{2RT_d}\right\} \quad \text{at } x=\infty, \end{aligned}\right\} \tag{2}$$

where R is the gas constant, n_u, n_d, u_u, u_d, T_u and T_d denote, respectively, the number density, velocity, and tempereture of the up-stream and down-stream equilibium states of the shock wave, and $\mathbf{i}$ is the unit vector in the x-direction. Therefore, some appropriate approximation should be introduced. It may be said that the validity of the theory of the one-dimensional neutral shock wave structure depends on how well one approximates Eq. (1) to the physical situations.

For the state of small departure from the local thermodynamic equilibrium, the usual Navier-Stokes equations (with the values of the viscosity coefficient μ and the thermal conductivity λ) may be obtained by the Chapman-Enskog expansion of f about the local equilibrium states and by taking the first approximation, which are written as follows;

$$\frac{d(\rho u)}{dx}=0, \tag{3}$$

$$\frac{d(\rho u^2)}{dx}+\frac{dp}{dx}-\frac{d\tau}{dx}=0, \tag{4}$$

$$\frac{d}{dx}\left\{u\left(e+\frac{1}{2}u^2+\frac{p}{\rho}\right)\right\}-\frac{d(u\tau)}{dx}+\frac{dq}{dx}=0, \tag{5}$$

where ρ represents density, p the pressure, e the specific internal energy ($e=c_vT$), $\tau=\mu\frac{du}{dx}$ and $q=-\lambda\frac{dT}{dx}$. The profiles of density, temperature, velocity, pressure etc. across the shock wave are obtained by taking into consideration the appropriate temperature dependencies of μ and λ, and by numerically integrating Eqs. (3)-(5)[2]. Recently, the numerical calculations[14] have been carried out by assuming the more appropriate temperature dependencies of μ and λ, but the results do not give any qualitative change from those obtained in Ref. 2.

The experimental values cannot be sufficiently reproduced by the Navier-Stokes approach for higher Mach numbers. Therefore, Mott-Smith[3] resorted to Eq. (1) and made the calculation assuming that the distribution function within the shock front would be expressed by the superposition of the equilibrium distribution functions at the up- and down-stream of the shock wave. Namely,

$$f(x,\mathbf{c})=b_0(x)f_u+a_0(x)f_d, \tag{6}$$

where $b_0(\infty)=a_0(-\infty)=0$, $b_0(-\infty)=n_u$ and $a_0(\infty)=n_d$ by the boundary conditions given by Eq. (2).

Substituting Eq. (6) into Eq. (1) and calculating the proper moment equations, one can determine $b_0(x)$ and $a_0(x)$, and with that the number density $n(x)$, for example, will be obtained by

$$n(x)=\int f(x,\mathbf{c})d\mathbf{c}=b_0(x)+a_0(x). \tag{7}$$

While this method gives good results judging from the comparison of them with the experimentally measured density profiles for Mach numbers greater than about 2, 4, errors become appreciable for lower Mach numbers.

Recently, several proposals have been made to improve the Mott-Smith method at low Mach numbers, e. g., to superpose Eq. (6) some additional proper Gaussian distribution functions[15], or to adopt the ellipsoidal distribution function[16),17], or to expand f by taking the bimodal distribution function Eq. (6) as a weighting function[18]. Furthermore, various other methods have been proposed, including two fluid model theory[19] and the method to numerically calculate the distribution function by the Krook model[20),21]. But in the latter method, the dissipation mechanisms seem not to be correctly taken into considerations[17].

Anyway, the generalized discussions have not been exercised of each method so far, and these and related topics will be discussed in **VI** after the present treatment will be shown.

The present author expanded the distribution function f in terms of the Hermite polynomial, the downstream equilibrium distribution function taken to be the weighting function. By properly truncating the expansion, the shock wave structure has been investigated.

II. Distribution Function and Fundamental Equations

Boltzmann equation Eq. (1) is used to describe the one-dimensional, steady neutral shock wave structure under the boundary conditions of Eq. (2).

As the convergence is not sufficient if a distribution function is expanded within the shock front about the local or the upstream equilibrium distribution function[15], we expand it about the downstream equilibrium distribution function. As the equilibrium distribution function is the Gaussian, it will be appropriate to expand f in terms of the Hermite polynomial as follows:

$$f=f_d \sum_{\rho\mu\nu} \frac{1}{\rho!\mu!\nu!} a_{\rho\mu\nu}(x) H_{\rho\mu\nu}, \tag{8}$$

where $H_{\rho\mu\nu}$ represents the three-dimensional Hermite polynomial, i.e.,

$$H_{\rho\mu\nu}=H_\rho\left(\frac{u-u_d}{v_d}\right)H_\mu\left(\frac{v}{v_d}\right)H_\nu\left(\frac{w}{v_d}\right), \tag{9}$$

$$H_\rho(\xi)=(-1)^\rho e^{\xi^2/2}\frac{d^\rho}{d\xi^\rho}e^{-\xi^2/2}, \tag{10}$$

and $v_d=\sqrt{RT_d}$.

As Eq. (8) is the expansion of f about the downstream distribution function, it becomes very complicated form when the upstream boundary condition will be taken into this expansion. Therefore, instead of f, the function $f-b_{000}(x)f_u$ is expanded about the downstream equilibrium distribution function f_d and the boundary conditions are made to be easily taken into the formulation, namely;

$$f-b_{000}(x)f_u=f_d\sum_{\rho\mu\nu}\frac{1}{\rho!\mu!\nu!}a_{\rho\mu\nu}(x)H_{\rho\mu\nu}. \tag{11}$$

With this formulation, the boundary conditions of Eq. (11) become

$$\left.\begin{aligned} &b_{000}(-\infty)=n_u \quad , \quad b_{000}(\infty)=0 \quad , \\ &a_{\rho\mu\nu}(-\infty)=0 \quad , \quad a_{\rho\mu\nu}(\infty)=0 \qquad \textit{besides } a_{000}(\infty)=n_d. \end{aligned}\right\} \tag{12}$$

In order to determine the coefficients of expansion Eq. (11) under these boundary conditions, the moment equations of Eq. (1) is used, which describe the transport of some arbitrary dynamical variable $\Phi(\mathbf{c})$;

$$\int u\Phi(\mathbf{c})\frac{\partial f}{\partial x}d\mathbf{c}=\iiiint \Phi(\mathbf{c})\,(f_1'f'-f_1f)\,gbdbd\varepsilon d\mathbf{c}_1 d\mathbf{c}. \tag{13}$$

First, the conservation equations are obtained by taking $\Phi(\mathbf{c})=1$, u, v, w, and $\mathbf{c}^2$ which are conserved at the collision;

$$u_u\frac{db_{000}}{dx}+u_d\frac{da_{000}}{dx}+v_d\frac{da_{100}}{dx}=0, \tag{14}$$

$$\left.\begin{aligned}&(u_u^2+RT_u)\frac{db_{000}}{dx}+(u_d^2+RT_d)\frac{da_{000}}{dx}+2u_dv_d\frac{da_{100}}{dx}+v_d^2\frac{da_{200}}{dx}=0,\\&u_d\frac{da_{010}}{dx}+v_d\frac{da_{110}}{dx}=u_d\frac{da_{001}}{dx}+v_d\frac{da_{101}}{dx}=0,\end{aligned}\right\} \tag{15}$$

$$\begin{aligned}&u_u(u_u^2+5RT_u)\frac{db_{000}}{dx}+u_d(u_d^2+5RT_d)\frac{da_{000}}{dx}+v_d(3u_d^2+5v_d^2)\frac{da_{100}}{dx}\\&+u_dv_d^2\left(3\frac{da_{200}}{dx}+\frac{da_{020}}{dx}+\frac{da_{002}}{dx}\right)+v_d^3\left(\frac{da_{300}}{dx}+\frac{da_{120}}{dx}+\frac{da_{102}}{dx}\right)=0.\end{aligned} \tag{16}$$

Integrating Eqs. (14)-(16) under the given boundary conditions, Eq. (12), one obtains,

$$u_da_{010}+v_da_{110}=u_da_{001}+v_da_{101}=0, \tag{17}$$

$$\frac{b_{000}(x)}{b_{000}(-\infty)}+\frac{a_{000}(x)}{a_{000}(\infty)}+\frac{v_d}{u_d}\cdot\frac{a_{100}(x)}{a_{000}(\infty)}=1, \tag{18}$$

$$\frac{b_{000}(x)}{b_{000}(-\infty)}+\frac{a_{000}(x)}{a_{000}(\infty)}+\frac{2u_dv_d}{u_d^2+v_d^2}\cdot\frac{a_{100}(x)}{a_{000}(\infty)}+\frac{v_d^2}{u_d^2+v_d^2}\cdot\frac{a_{200}(x)}{a_{000}(\infty)}=1, \tag{19}$$

$$\begin{aligned}&\frac{b_{000}(x)}{b_{000}(-\infty)}+\frac{a_{000}(x)}{a_{000}(\infty)}+\frac{v_d(3u_d^2+5v_d^2)}{u_d(u_d^2+5v_d^2)}\cdot\frac{a_{100}(x)}{a_{000}(\infty)}\\&\quad+\frac{v_d^2}{u_d^2+5v_d^2}\cdot\frac{3a_{200}(x)+a_{020}(x)+a_{002}(x)}{a_{000}(\infty)}\\&\quad+\frac{v_d^3}{u_d(u_d^2+5v_d^2)}\cdot\frac{a_{300}(x)+a_{120}(x)+a_{102}(x)}{a_{000}(\infty)}=1,\end{aligned} \tag{20}$$

In the following, we set $b_{000}(x)=b_0(x)$, $a_{000}(x)=a_0(x)$, and $a_{100}(x)=a_1(x)$, as $a_{101}(x)=a_{110}(x)=a_{001}(x)=a_{101}(x)=0$ which will be shown later.

By putting $a_1(x)=a_{200}(x)=\cdots\cdots=0$ in Eq. (11), the usual Mott-Smith bimodal distribution function[3] is obtained, and in this sense the present method may be thought of as the extension of Mott-Smith's treatment. By putting $a_1(x)=a_{200}(x)=\cdots\cdots=0$, Eqs. (18)-(20) become the indentical form,

$$\frac{b_0(x)}{b_0(-\infty)}+\frac{a_0(x)}{a_0(\infty)}=1, \tag{21}$$

then the characteristics of the mass, momentum and energy transports are not independently taken into this formulation, while Eqs. (18)-(20) are independent set of equations in the present method.

Using the boundary conditions of Eq. (12), in Eqs. (18)-(20), one obtains,

$$\left.\begin{aligned}&u_ub_0(-\infty)=u_da_0(\infty),\\&(u_u^2+RT_u)b_0(-\infty)=(u_d^2+RT_d)a_0(\infty),\\&u_u(u_u^2+5RT_u)b_0(-\infty)=u_d(u_d^2+5RT_d)a_0(\infty),\end{aligned}\right\} \tag{22}$$

and from these equations, the following usual Rankine-Hugoniot relations are obtained for the equilibrium values at the up- and down-stream of the shock

wave:

$$\left.\begin{aligned}&\frac{u_d}{u_u}=\frac{b_0(-\infty)}{a_0(\infty)}=\frac{1}{4}\left(1+\frac{3}{\mathrm{M}^2}\right)\equiv\varepsilon,\\&\frac{T_d}{T_u}=\frac{\varepsilon(4-\varepsilon)}{4\varepsilon-1},\end{aligned}\right\}\tag{23}$$

in which we put

$$\mathrm{M}^2=\frac{u_u^2}{\frac{5}{3}RT_u},\tag{24}$$

assuming a monatomic gas.

The method described below is to make the necessary moment equations from Eq. (13) to determine the coefficients of the expansion Eq. (11), and from it the state within the shock front will be known. It is, therefore, necessary to truncate Eq. (11) by some physically meaningful method in order to close the formulation. While, it is easy to show that at least three terms should be added to the Mott-Smith approximation to make Eqs. (18)-(20) independent. In the following, five terms are retained among those appearing in Eqs. (18)-(20). Two more equations are needed for the five undetermined coefficients and three equations are given by Eqs. (18)-(20). As the two equations, $\Phi(\mathbf{c})=u^2$ and u^3 are taken. The dissipation mechanisms within the shock front are determined by the moments of the collision terms of these dynamical variables which are not conserved at the collisions.

It is difficult at this stage to determine which of the coefficients in Eqs. (18)-(20) should be retained. First, $a_1(x)$ and $a_{200}(x)$ must be taken to make Eqs. (18) and (19) independent. The calculations are carried out by retaining as one more additional term, $a_{020}(x)+a_{002}(x)$ (one can put $a_{020}(x)=a_{002}(x)$ without the loss of generality) or $a_{300}(x)$. The physical meaning and the effects of these choices on the results will be discussed later.

For these two types of truncation, $a_{200}(x)$ and $a_{020}(x)+a_{002}(x)$ or $a_{200}(x)$ and $a_{300}(x)$ are given as a function of $a_1(x)$, from Eqs. (18)-(20), as follows;

(i) case of adopting $a_{020}(x)+a_{002}(x)$:

$$\left.\begin{aligned}&a_{200}(x)=-\frac{u_d^2-v_d^2}{u_dv_d}a_1(x)=\frac{4-6\varepsilon}{\sqrt{5\varepsilon(4-\varepsilon)}}a_1(x),\\&a_{020}(x)+a_{002}(x)=\frac{u_d^2-3v_d^2}{u_dv_d}a_1(x)=\frac{4(2\varepsilon-3)}{\sqrt{5\varepsilon(4-\varepsilon)}}a_1(x),\end{aligned}\right\}\tag{25}$$

(ii) case of adopting $a_{300}(x)$:

$$\left.\begin{aligned}&a_{200}(x)=-\frac{u_d^2-v_d^2}{u_dv_d}a_1(x)=\frac{4-6\varepsilon}{\sqrt{5\varepsilon(4-\varepsilon)}}a_1(x),\\&a_{300}(x)=\frac{u_d^2-3v_d^2}{v_d^2}a_1(x)=-\frac{4(2\varepsilon-3)}{\varepsilon-4}a_1(x).\end{aligned}\right\}\tag{26}$$

III. Calculation for Maxwell Molecules

In calculating the collision term of Eq. (13), the Maxwellian repulsive force is assumed as the interparticle force ($F=K/r^5$). In the following are shown the fundamental equations for the cases in which $a_{020}(x)+a_{002}(x)$ or $a_{300}(x)$ is retained in the formulation. (For the collision moments, see Appendix.)

(i) $a_{020}(x)+a_{002}(x)$:

$\Phi(\mathbf{c})=u^2$;

$$u_u(u_u^2+3RT_u)\frac{db_0}{dx}+u_d(u_d^2+3\mathrm{RT}_d)\frac{da_0}{dx}$$

$$+3v_d(u_d^2+v_d^2)\frac{da_1}{dx}+3u_dv_d^2\frac{da_{200}}{dx}$$

$$=\pi\left(\frac{2K}{m}\right)^{1/2}\Big[b_0a_0\{-A_2(u_u^2+u_d^2-2u_uu_d)\}+b_0a_1\{2A_2v_d(u_u-u_d)\}$$

$$+(b_0+a_0)\left(-a_{200}+\frac{a_{020}+a_{002}}{2}\right)(A_2v_d^2)+(a_1)^2(A_2v_d^2)\Big], \tag{27}$$

$\Phi(\mathbf{c})=u^3$;

$$\{3(RT_u)^2+6u_u^2RT_u+u_u^4\}\frac{db_0}{dx}+\{3(RT_d)^2+6u_d^2RT_d+u_d^4\}\frac{da_0}{dx}$$

$$+4u_dv_d(u_d^2+3v_d^2)\frac{da_1}{dx}+6v_d^2(u_d^2+v_d^2)\frac{da_{200}}{dx}$$

$$=\pi\left(\frac{2K}{m}\right)^{1/2}\Big[b_0a_0\left\{\frac{3}{2}A_2(u_u-u_d)(-u_u^2+u_d^2-2RT_u+2RT_d)\right\}$$

$$+b_0a_1\left\{\frac{3}{2}A_2v_d(u_u^2-3u_d^2+2u_uu_d+2RT_u-2RT_d)\right\}$$

$$+b_0a_{200}\left\{\frac{3}{2}A_2v_d^2(u_u-3u_d)\right\}$$

$$+b_0(a_{020}+a_{002})\left\{\frac{3}{4}A_2v_d^2(u_u+u_d)\right\}$$

$$+a_0a_{200}\{-3A_2u_dv_d^2\}+a_0(a_{020}+a_{002})\left\{\frac{3}{2}A_2u_dv_d^2\right\}$$

$$+(a_1)^2\{3A_2u_dv_d^2\}+a_1a_{200}\left\{\frac{3}{2}A_2v_d^3\right\}$$

$$+a_1(a_{020}+a_{002})\left\{\frac{3}{4}A_2v_d^3\right\}\Big], \tag{28}$$

(ii) $a_{300}(x)$:

$\Phi(\mathbf{c})=u^2$;

$$u_u(u_u^2+3RT_u)\frac{db_0}{dx}+u_d(u_d^2+3RT_d)\frac{da_0}{dx}$$
$$+3v_d(u_d^2+v_d^2)\frac{da_1}{dx}+3u_dv_d^2\frac{da_{200}}{dx}+v_d^3\frac{da_{300}}{dx}$$
$$=\pi\left(\frac{2K}{m}\right)^{1/2}\Big[b_0a_0\{-A_2(u_u^2+u_d^2-2u_uu_d)\}+b_0a_1\{2A_2v_d(u_u-u_d)\}$$
$$+(b_0+a_0)a_{200}\{-A_2v_d^2\}+(a_1)^2(A_2v_d^2)\Big], \tag{29}$$

$\Phi(\mathbf{c})=u^3$;

$$\{3(RT_u)^2+6u_u^2RT_u+u_u^4\}\frac{db_0}{dx}+\{3(RT_d)^2+6u_d^2RT_d+u_d^4\}\frac{da_0}{dx}$$
$$+4u_dv_d(u_d^2+3v_d^2)\frac{da_1}{dx}+6v_d^2(u_d^2+v_d^2)\frac{da_{200}}{dx}+4u_dv_d^3\frac{da_{300}}{dx}$$
$$=\pi\left(\frac{2K}{m}\right)^{1/2}\Big[b_0a_0\left\{\frac{3}{2}A_2(u_u-u_d)(-u_u^2+u_d^2-2RT_u+2RT_d)\right\}$$
$$+b_0a_1\left\{\frac{3}{2}A_2v_d(u_u^2-3u_d{}^2+2u_uu_d+2RT_u-2RT_d)\right\}$$
$$+b_0a_{200}\left\{\frac{3}{2}A_2v_d^2(u_u-3u_d)\right\}+a_0a_{200}\{-3A_2u_dv_d^2\}$$
$$+(a_1)^2\{3A_2u_dv_d^2\}+a_1a_{200}\left\{\frac{3}{2}A_2v_d^3\right\}$$
$$+(b_0+a_0)a_{300}\left\{-\frac{3}{2}A_2v_d^3\right\}\Big], \tag{30}$$

where $A_2=0.436$ for the Maxwell molecules[13].

Eliminating $a_{200}(x)$ and $a_{020}(x)+a_{002}(x)$ or $a_{200}(x)$ and $a_{300}(x)$ by using Eq. (25) or (26), respectively, and making use of Eq. (18), one obtains the equations describing α_0 and β_0. Here the following dimensionless quantities are introduced besides Eq. (23);

$$\left.\begin{aligned}\alpha_0&=\frac{a_0(x)}{a_0(\infty)}\ ,\qquad \beta_0=\frac{b_0(x)}{b_0(-\infty)}\ ,\\ \xi&=\frac{x}{l_a}\ ,\qquad l_a=\frac{u_u}{\pi b_0(-\infty)}\left(\frac{m}{2K}\right)^{1/2}.\end{aligned}\right\} \tag{31}$$

With the above dimensionless expressions, it is easy to see that $\alpha_0(-\infty)=0$, $\beta_0(-\infty)=1$ and $\alpha_0(\infty)=1$, $\beta_0(\infty)=0$, and l_a is related to the upstream mean free path $\lambda(-\infty)$ based on the viscosity by

$$\lambda(-\infty)=l_a\frac{2\left\{2(4\varepsilon-1)\right\}^{1/2}}{\sqrt{5}\,A_2\Gamma\left(\frac{7}{2}\right)}\ . \tag{32}$$

The equations for α_0 and β_0 are as follows:

(i) $a_{020}(x)+a_{002}(x)$:

$$\begin{aligned}
&(-110\varepsilon^4+300\varepsilon^3-330\varepsilon^2+200\varepsilon-60)\frac{d\beta_0}{d\xi}\\
&\quad=15A_2(\varepsilon^2+12\varepsilon-14)\\
&\qquad+\alpha_0\left(-30A_2\frac{4\varepsilon^3-5\varepsilon^2+8\varepsilon-8}{\varepsilon}\right)+\beta_0\left\{-15A_2(18\varepsilon^3-45\varepsilon^2+56\varepsilon-31)\right\}\\
&\qquad+\alpha_0\beta_0\left\{15A_2\frac{7\varepsilon^4-4\varepsilon^3-16\varepsilon^2+28\varepsilon-17}{\varepsilon}\right\}\\
&\qquad+\alpha_0^2\left\{15A_2\frac{7\varepsilon^3-22\varepsilon^2+30\varepsilon-16}{\varepsilon}\right\}+\beta_0^2\left\{15A_2(18\varepsilon^3-46\varepsilon^2+44\varepsilon-17)\right\},
\end{aligned} \tag{33}$$

$$\begin{aligned}
&-\varepsilon(-110\varepsilon^4+300\varepsilon^3-330\varepsilon^2+200\varepsilon-60)\frac{d\alpha_0}{d\xi}\\
&\quad=5A_2(16\varepsilon^3+9\varepsilon^2-30\varepsilon+2)\\
&\qquad+\alpha_0\left(10A_2\frac{-9\varepsilon^4+2\varepsilon^3-3\varepsilon^2+12\varepsilon+1}{\varepsilon}\right)\\
&\qquad+\beta_0\left\{-\frac{5}{2}A_2(81\varepsilon^4-188\varepsilon^3+252\varepsilon^2-168\varepsilon+11)\right\}\\
&\qquad+\alpha_0\beta_0\left(\frac{5}{2}A_2\frac{4\varepsilon^5+55\varepsilon^4-148\varepsilon^3+182\varepsilon^2-112\varepsilon+7}{\varepsilon}\right)\\
&\qquad+\alpha_0^2\left(5A_2\frac{2\varepsilon^4-13\varepsilon^3+36\varepsilon^2-26\varepsilon-2}{\varepsilon}\right)\\
&\qquad+\beta_0^2\left\{\frac{5}{2}A_2(81\varepsilon^4-220\varepsilon^3+234\varepsilon^2-108\varepsilon+7\right\}.
\end{aligned} \tag{34}$$

(ii) $a_{300}(x)$:

$$\begin{aligned}
&-2(\varepsilon^2-1)\frac{d\beta_0}{d\xi}=5A_2+\alpha_0\left(-4A_2\frac{\varepsilon+1}{\varepsilon}\right)+\beta_0\left\{-4A_2(\varepsilon+1)\right\}\\
&\qquad+\alpha_0\beta_0\left(-A_2\frac{\varepsilon^2-8\varepsilon+1}{\varepsilon}\right)+\alpha_0^2\left(-A_2\frac{\varepsilon-4}{\varepsilon}\right)+\beta_0^2\left\{A_2(4\varepsilon-1)\right\},
\end{aligned} \tag{35}$$

$$2\varepsilon(\varepsilon^2-1)(-29\varepsilon^2+72\varepsilon-24)\frac{d\alpha_0}{d\xi}=5A_2(-22\varepsilon^3+54\varepsilon^2-6\varepsilon-7)$$
$$+\alpha_0\left\{-2A_2\frac{(\varepsilon+1)(-41\varepsilon^3+96\varepsilon^2-15\varepsilon-2)}{\varepsilon}\right\}$$
$$+\beta_0\left\{\frac{A_2}{2}(\varepsilon+1)(179\varepsilon^3-399\varepsilon^2+45\varepsilon+23)\right\}$$
$$+\alpha_0\beta_0\left\{\frac{A_2}{2}\cdot\frac{56\varepsilon^5-499\varepsilon^4+824\varepsilon^3-184\varepsilon^2-16\varepsilon+47}{\varepsilon}\right\}$$
$$+\alpha_0^2\left\{A_2\frac{(\varepsilon-4)(28\varepsilon^3-48\varepsilon^2+1)}{\varepsilon}\right\}$$
$$+\beta_0^2\left\{\frac{A_2}{2}(-179\varepsilon^4+440\varepsilon^3-186\varepsilon^2-8\varepsilon+47)\right\}. \qquad (36)$$

By solving these non-linear differential equations Eqs. (33), (34) or Eqs. (35), (36), one obtains α_0, β_0, and from it the distribution function f. By the way, $(\alpha_0, \beta_0)=(0, 1)$ and $(1, 0)$, corresponding to the up- and down-stream equilibrium state, respectively, are the singular points for both Eqs. (33), (34) and Eqs. (35), (36). While both singularities are the saddle points for Eqs. (33), (34) at $M\geq 2.05$ and there is no integral curves joining these singular points, for Eqs. (35), (36) is $(1, 0)$ the stable nodal point and $(0, 1)$ the saddle point for $1\leq M\leq 2.26$ and the types of the two singularities are reversed for $M\geq 2.27$, but the solutions exist for any Mach number $M>1.0$.

To show the state near the singular points and the solution curves, the integral curves are shown in Fig. 1 for $M=2.0$ and Fig. 2 for $M=5.0$ which are obtained by integrating Eqs. (35) and (36) by the usual Runge-Kutta-Gill method. The curves labelled A and B in these figures are the zero points of A and B respectively when we put $d\beta_0/d\alpha_0=B/A$. Several solution curves are given in Fig. 3 joining the two singular points for the case of $a_{300}(x)$. The straight line joining $(1, 0)$ and $(0, 1)$ is obtained by putting $a_1(x)=a_{200}(x)=\cdots\cdots=0$ in Eq. (11), and it is the Mott-Smith result. It is easy to see the degree of the correction of the distribution function from the Mott-Smith bimodal one.

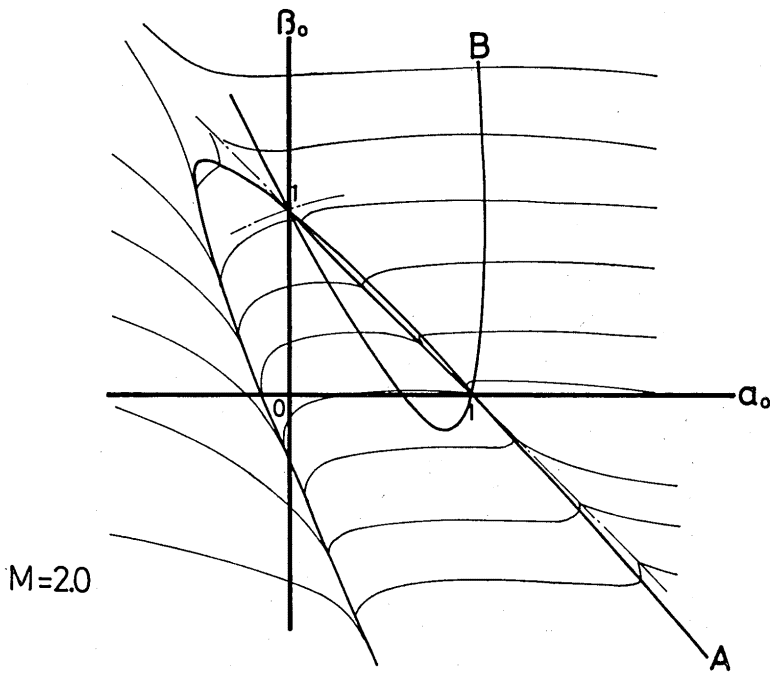

Fig. 1. Integral curves, a_{300}, M=2.0.

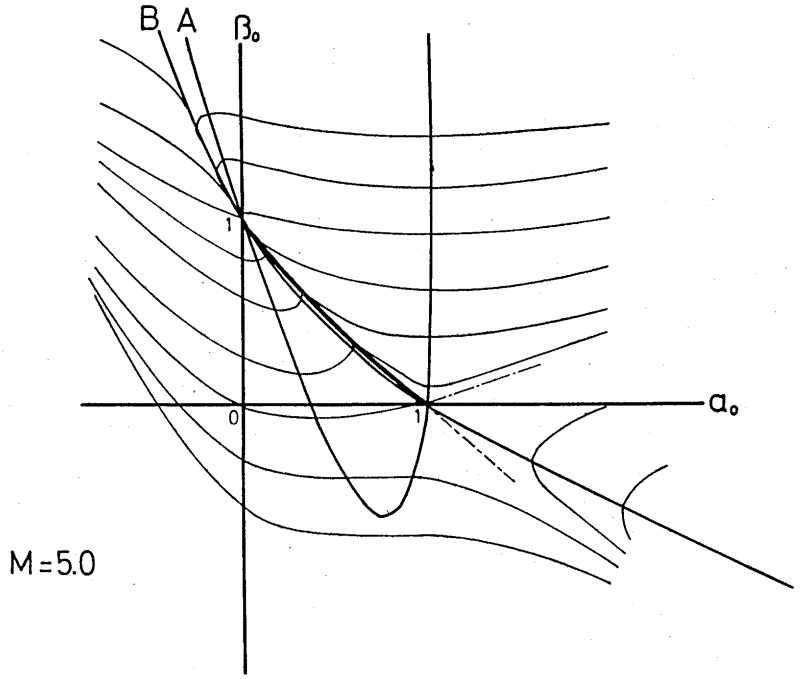

Fig. 2. Integral curves, a_{300}, M=5.0.

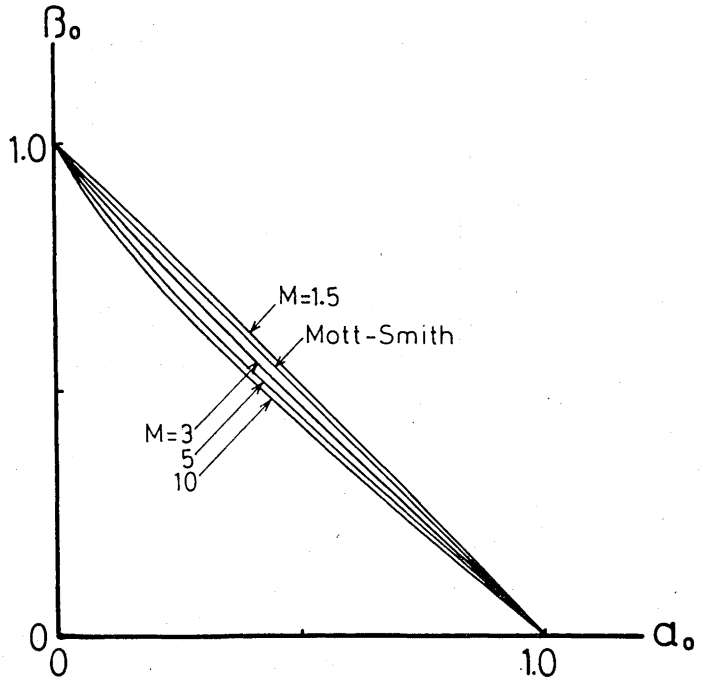

Fig. 3. Solution curves, a_{300}.

IV. Definition of the Thermodynamic Variables and Their Profiles

The dependencies of α_0 and β_0 on ξ are known from one of Eq. (35) or (36), and the solution curves like Fig. 3. Then by using Eqs. (18) and (26), it is possible to know the dependency of the distribution function f on ξ. The process is indentical for the case of adopting $a_{020}(x)+a_{002}(x)$ by using Eqs. (18), (25), (33) and (34). With this knowledge of f, it is possible to know local thermodynamic variables by taking the proper moment of this distribution function.

The local number density $n(x)$, flow spead $u_0(x)$, temperature $T(x)$, pressure tensor $\mathbf{P}(x)$ and heat flux $q(x)$ are defined as follows;

$$n(x) \equiv \int f(x, \mathbf{c})\, d\mathbf{c} = b_0(x) + a_0(x), \tag{37}$$

$$u_0(x) \equiv \frac{1}{n(x)} \int u f(x, \mathbf{c})\, d\mathbf{c}$$

$$= \frac{1}{n(x)} \left\{ u_u b_0(x) + u_d a_0(x) + v_d a_1(x) \right\}, \tag{38}$$

$$T(x) \equiv \frac{1}{3Rn(x)} \int \left\{ \mathbf{c} - \mathbf{i} u_0(x) \right\}^2 f(x, \mathbf{c})\, d\mathbf{c}$$

$$= \frac{1}{3Rn(x)} \Big[b_0(x) \{ (u_0(x) - u_u)^2 + 3RT_u \}$$

$$+ a_0(x) \{ (u_0(x) - u_d)^2 + 3RT_d \}$$

$$- 2a_1(x) \{ u_0(x) - u_d \} v_d$$

$$+ \{ a_{200}(x) + a_{020}(x) + a_{002}(x) \} v_d^2 \Big], \tag{39}$$

$$\mathbf{P}(x) \equiv \int m \{ \mathbf{c} - \mathbf{i} u_0(x) \} \{ \mathbf{c} - \mathbf{i} u_0(x) \} f(x, \mathbf{c})\, d\mathbf{c}, \tag{40}$$

$$q(x) \equiv \int \frac{m}{2} (\mathbf{c} - \mathbf{i} u_0)^2 (u - u_0) f(x, \mathbf{c})\, d\mathbf{c}$$

$$= \frac{m}{2} \Big[b_0(x) \{ -(u_0 - u_u)^3 - 5RT_u (u_0 - u_u) \}$$

$$+ a_0(x) \{ -(u_0 - u_d)^3 - 5RT_d (u_0 - u_d) \}$$

$$+ a_1(x) \{ 3(u_0 - u_d)^2 + 5RT_d \} v_d$$

$$- \{ 3a_{200}(x) + a_{020}(x) + a_{002}(x) \} (u_0 - u_d) v_d^2$$

$$+ a_{300}(x) v_d^3 \Big]. \tag{41}$$

where Eq. (11) is used to get the last expressions.

The each quantity in the right-hand side of Eqs. (37)-(41) has the different value depending on which of $a_{020}(x) + a_{002}(x)$ or $a_{300}(x)$ is retained and it is possible to write them only by $a_0(x)$ and $b_0(x)$ by using Eqs. (18), (25) or Eqs. (18), (26) for each case.

Using the non-dimensionalized expressions of Eqs. (23) and (31), Eqs. (37), (38), (39) and (41) may be written as follows (the pressure tensor, given by Eq. (40), will be described in the next section);

(i) $a_{020}(x) + a_{002}(x)$:

$$\tilde{n}_\varepsilon \equiv \frac{n(x)}{n(-\infty)} = \beta_0(\xi) + \frac{1}{\varepsilon} \alpha_0(\xi), \tag{42}$$

$$\tilde{u}_\varepsilon \equiv \frac{u_0(x)}{u_u} = \frac{n(-\infty)}{n(x)} = \frac{1}{\tilde{n}_\varepsilon}, \tag{43}$$

$$\tilde{T}_\varepsilon \equiv \frac{T(x)}{T_u} = \frac{RT}{u_u^2} \cdot \frac{u_u^2}{RT_u} = \frac{5}{4\varepsilon - 1} \tilde{T}, \tag{44}$$

$$\tilde{T} \equiv \frac{RT(x)}{u_u^2}$$

$$= \frac{\beta_0}{3\tilde{n}_\varepsilon}\left\{(\tilde{u}_\varepsilon - 1)^2 + 2\tilde{u}_\varepsilon + 1\right\} + \frac{\alpha_0}{3\varepsilon\tilde{n}_\varepsilon}\left\{(\tilde{u}_\varepsilon - \varepsilon)^2 + 2\varepsilon\tilde{u}_\varepsilon + \varepsilon(4-3\varepsilon)\right\}$$

$$+ \frac{2}{3\tilde{n}_\varepsilon}\left\{\frac{6\varepsilon-4}{5} - \tilde{u}_\varepsilon\right\}, \tag{45}$$

$$\tilde{q}_\varepsilon \equiv \frac{q(x)}{mn(-\infty)u_u^3/2}$$

$$= \beta_0\Big[-(\tilde{u}_\varepsilon - 1)^3 - (4\varepsilon - 1)(\tilde{u}_\varepsilon - 1) - \{3(\tilde{u}_\varepsilon - \varepsilon)^2 + 2\varepsilon(\tilde{u}_\varepsilon - \varepsilon) + \varepsilon(4-\varepsilon)\}\Big]$$

$$+ \frac{\alpha_0}{\varepsilon}\Big[-(\tilde{u}_\varepsilon - \varepsilon)^3 - \varepsilon(4-\varepsilon)(\tilde{u}_\varepsilon - \varepsilon) - \varepsilon\{3(\tilde{u}_\varepsilon - \varepsilon)^2 + 2\varepsilon(\tilde{u}_\varepsilon - \varepsilon) + \varepsilon(4-\varepsilon)\}\Big]$$

$$+ \{3(\tilde{u}_\varepsilon - \varepsilon)^2 + 2\varepsilon(\tilde{u}_\varepsilon - \varepsilon) + \varepsilon(4-\varepsilon)\}. \tag{46}$$

(ii) $a_{300}(x)$:

$\tilde{n}_\varepsilon$, $\tilde{u}_\varepsilon$ and $\tilde{T}_\varepsilon$ take the same forms as Eqs. (42), (43) and (44), respectively, and $\tilde{T}$ and $\tilde{q}_\varepsilon$ are given as follows;

$$\tilde{T} = \frac{RT(x)}{u_u^2}$$

$$= \frac{\beta_0}{3\tilde{n}_\varepsilon}\left\{(\tilde{u}_\varepsilon - 1)^2 + 2\tilde{u}_\varepsilon + \frac{8\varepsilon-7}{5}\right\} + \frac{\alpha_0}{3\varepsilon\tilde{n}_\varepsilon}\left\{(\tilde{u}_\varepsilon - \varepsilon)^2 + 2\varepsilon\tilde{u}_\varepsilon + \frac{\varepsilon(-7\varepsilon+8)}{5}\right\}$$

$$+ \frac{2}{3\tilde{n}_\varepsilon}\left\{\frac{2}{5}(\varepsilon+1) - \tilde{u}_\varepsilon\right\}, \tag{47}$$

$$\tilde{q}_\varepsilon = \frac{q(x)}{mn(-\infty)u_u^3/2}$$

$$= \beta_0\left\{-(\tilde{u}_\varepsilon - 1)^3 - (4\varepsilon - 1)(\tilde{u}_\varepsilon - 1) - \frac{4\varepsilon}{5}(2\varepsilon - 3) - \frac{6(3\varepsilon-2)}{5}(\tilde{u}_\varepsilon - \varepsilon)\right\}$$

$$+ \frac{\alpha_0}{\varepsilon}\left\{-(\tilde{u}_\varepsilon - \varepsilon)^3 - \varepsilon(4-\varepsilon)(\tilde{u}_\varepsilon - \varepsilon) - \frac{4\varepsilon^2}{5}(2\varepsilon - 3) - \frac{6\varepsilon(3\varepsilon-2)}{5}(\tilde{u}_\varepsilon - \varepsilon)\right\}$$

$$+ \left\{\frac{4\varepsilon}{5}(2\varepsilon - 3) + \frac{6(3\varepsilon-2)}{5}(\tilde{u}_\varepsilon - \varepsilon)\right\}. \tag{48}$$

Furthermore, the gradient of the average velocity $\tilde{u}_\varepsilon$ can be calculated by

$$\frac{d\tilde{u}_\varepsilon}{d\xi} = -\frac{1}{\tilde{n}_\xi^2}\frac{d\tilde{n}_\varepsilon}{d\xi} = -\frac{1}{\tilde{n}_\xi^2}\frac{d}{d\xi}\left(\beta_0 + \frac{\alpha_0}{\varepsilon}\right)$$

$$= -\frac{1}{\tilde{n}_\xi^2}\left\{B(\alpha_0, \beta_0, M) + \frac{1}{\varepsilon}A(\alpha_0, \beta_0, M)\right\}, \tag{49}$$

where we put

$$\frac{d\alpha_0}{d\xi}=A(\alpha_0, \beta_0 M), \qquad \frac{d\beta_0}{d\xi}=B(\alpha_0, \beta_0, M),$$

to express Eqs. (33) and (34) or Eqs. (35) and (36). The gradient of tempetature $\frac{d\tilde{T}_\xi}{d\xi}$ may similarly be obtainable but becomes to a more complicated form. As these macroscopic variables are easily obtained from the distribution function f, the numerical calculations are easy and the physical meanings become very clear.

A. Density Profiles

The experimental studies of the shock front structure have been limited to the measurements of the density profiles so far, because of the experimental difficulties to measure other quantities. Therefore, the theoretical density profiles are to be compared with those of the experimental observations in order to test the validity of theories. Then, in this section, the results for the density profiles will be described among the thermodynamic

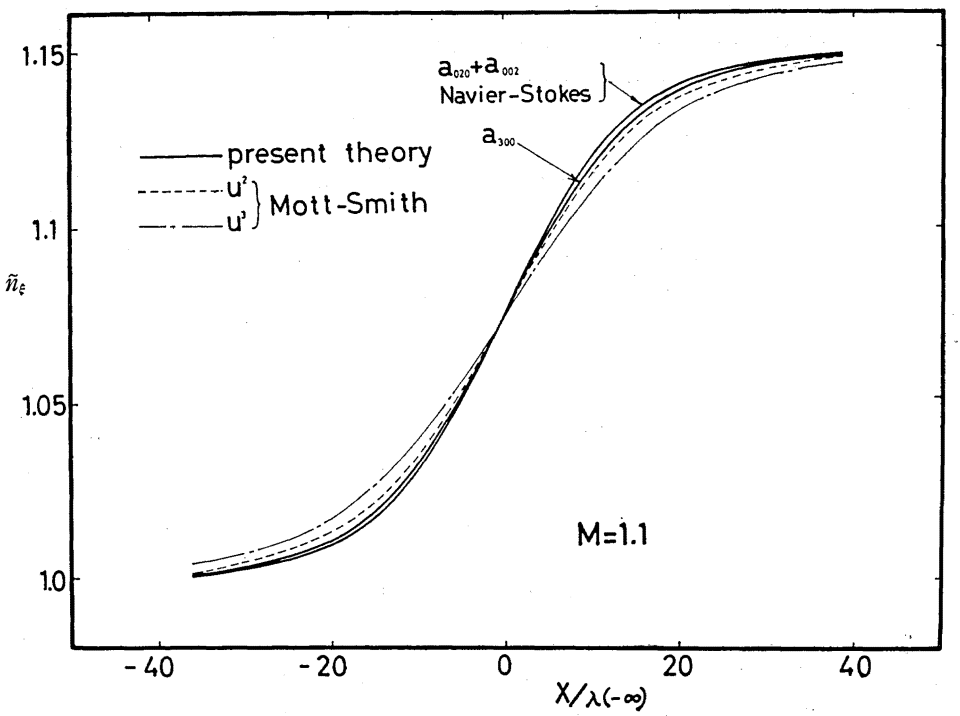

Fig. 4. Density profiles normalized to the upstream equilibrium value. The distance is measured in unit of the upstream mean free path. M=1.1.

variables defined above. As the thermodynamic states in the shock front are not wholly specified only by the density profiles, we cannot conclude, as will be discussed later, that the theory is correct in every respect only by the reason of the coincidence of the density profiles for the theoretical and experimental results.

In Figs. 4 and 5 are shown the density profiles for M=1.1 and 5.0 respectively, which were obtained from Eq. (42) using Eqs. (33) and (34) or Eqs. (35) and (36). In these figures are taken for the abscissas the distances along the shock passage normalized by the upstream mean free path defined by Eq. (32) and for the ordinates the number densities normalized by the upstream equilibrium value. The results using Mott-Smith u^2 and u^3 transport equations (for brevity, these will, hereafter, be denoted as M-S(u^2) and M-S (u^3) respectively) and using Navier-Stokes equations ('N-S approximation' will be used for this) are also shown in Figs. 4 and 5.

If the maximum-slope shock thickness based on the density profiles is defined by

$$\triangle=\frac{n(\infty)-n(-\infty)}{(dn/dx)_{max}}, \tag{50}$$

the relationship between $\lambda(-\infty)/\triangle$ and M can be obtained by the similar calculations performed for getting Figs. 4 and 5 for each Mach number. The

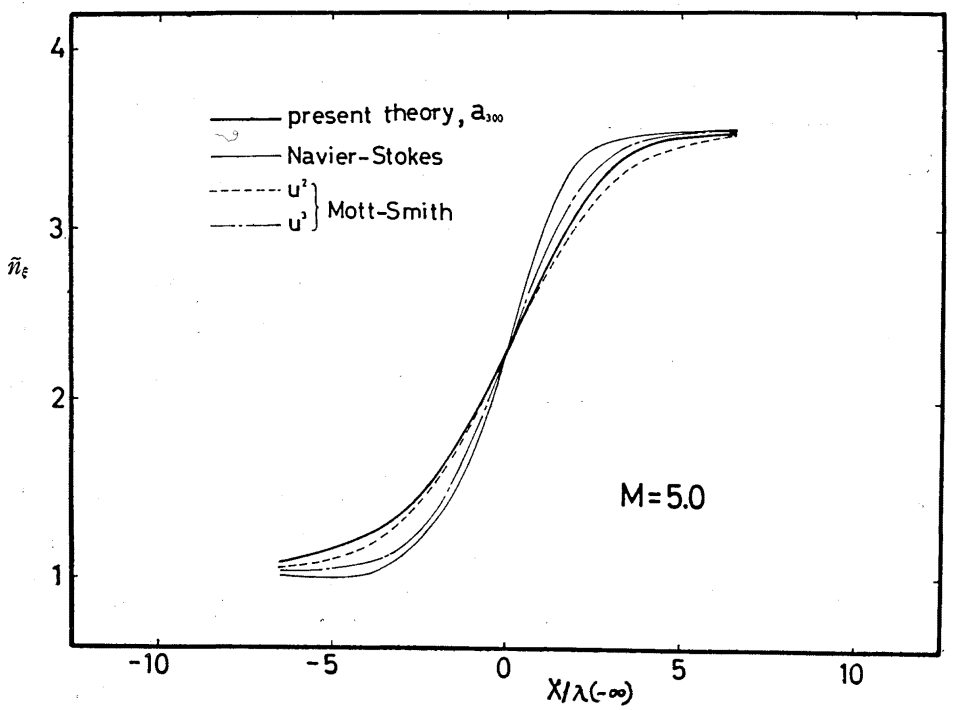

Fig. 5. Density profiles, M=5.0.

results are shown in Fig. 6 for $1 \leq M \leq 1.2$ and in Fig. 7 for $1 \leq M \leq 10$. As pointed out before, there is no solution for $M \geq 2.05$ for the case of adopting $a_{020}(x)+a_{002}(x)$, then this is not shown in Fig. 7. The results of Salwen et al.[15] are shown in Figs. 6 and 7 besides those of the present treatments, M-S (u^2), M-S(u^3) and N-S approximation.

As the shock profiles are different for each interparticle force law assumed, every result in Figs. 6 and 7 is calculated assuming the Maxwell molecules and the results for N-S approximation are obtained assuming that the viscosity has the linear relationship to temperature which is obtainable for the Maxwell molecules and which will be shown later. Meanwhile, Maxwell

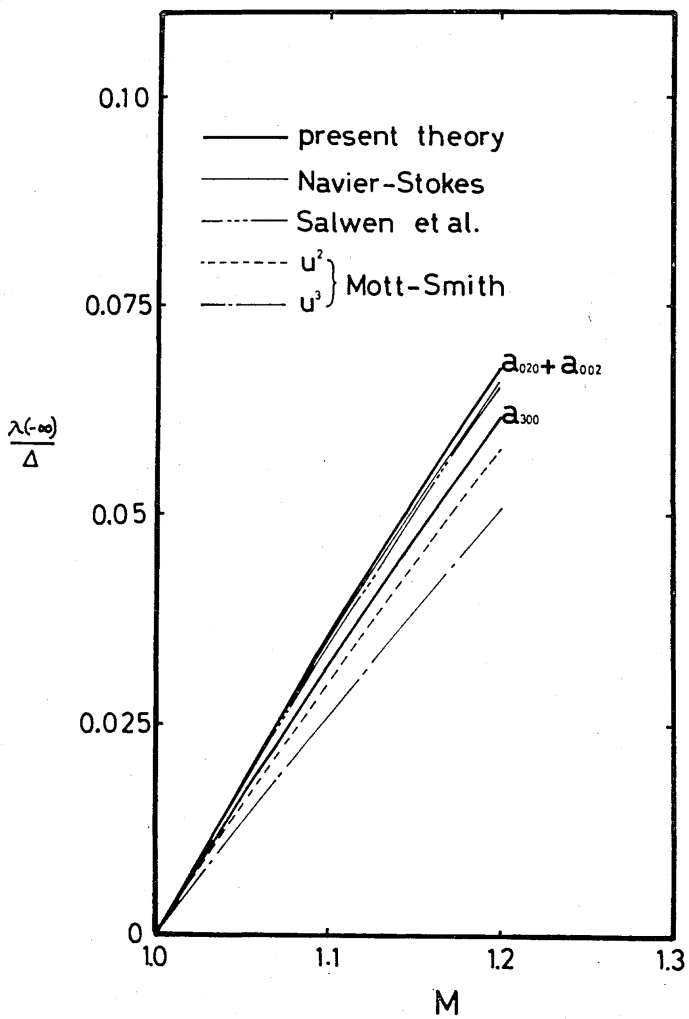

Fig. 6. Maximum-slope shock thickness ($1 \leq M \leq 1.2$).

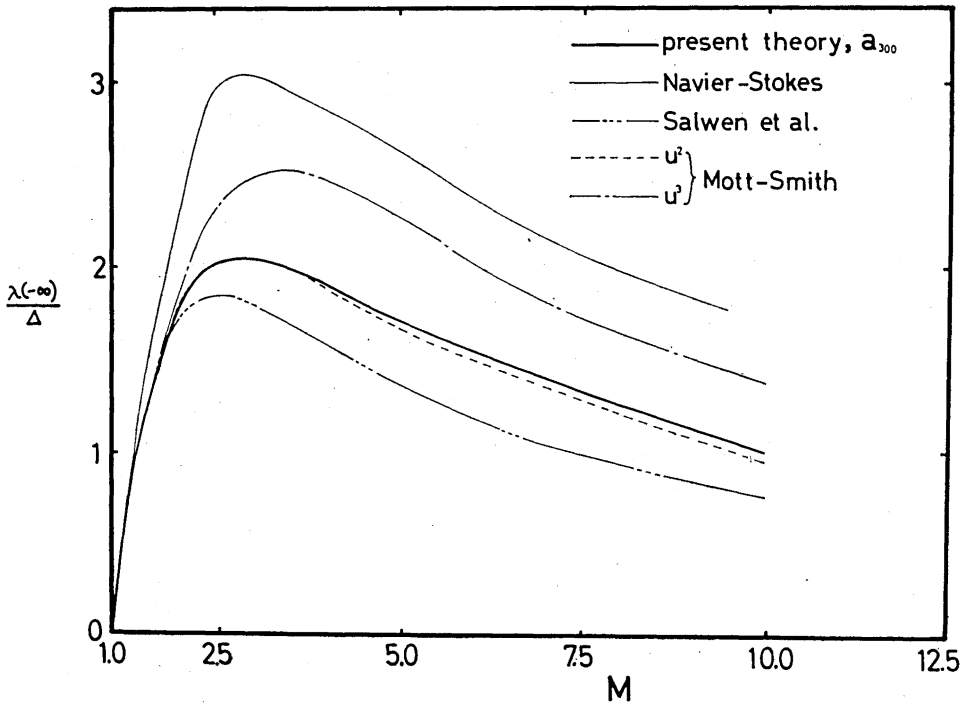

Fig. 7. Maximum-slope shock thickness ($1 \leq M \leq 10$).

repulsive force does not correctly describe the interparticle forces for the real gases like argon or helium, then it is impractical to directly compare the above calculations with the experiments and to know the validity of each approximation. On the other hand, as the N-S approximations give good results for low Mach numbers ($1 \leq M \leq 1.5$) and M-S (u^2) for higher Mach numbers ($M \geq 2.0$) by judging from the comparisons of the theories assuming a more realistic interparticle force law with experiments, these become one of the standards of comparison. In the following are shown the results for these two regions.

(i) $1 \leq M \leq 1.5$:

From Figs. 4 and 6, it is seen that the results of Salwen et al.[15] and $a_{020}(x)+a_{002}(x)$ of the present treatments almost coincide with those of the N-S approximation and these theories may be thought of as to give a good description of the phenomena for these low Mach number ranges. The results of $a_{300}(x)$ of the present treatments have been substantially improved from those of M-S(u^2) and M-S(u^3) but differ from those of the N-S approximation.

(ii) $2 < M < 10$:

As has been already mentioned, M-S(u^2) may give good results for the density profiles and it is seen from Figs. 5 and 7 that the results of $a_{300}(x)$ maintain the good feature of M-S(u^2). The results of N-S approximations and M-S(u^3) give too thin shock thicknesses and those of Salwen et al. too thick.

Further discussions will be given after other thermodynamic variables are shown.

B. Shock Profiles of Other Thermodynamic Variables

The calculated results for Eqs. (42), (43), (44), (45) and (47) are shown in Figs. 8 and 9 for M=1.1 and 5.0, respectively. For the abscissas are taken the same values as those of Figs. 4 and 5 and the origins have been chosen to be the points where each density profile has the maximum-slope.

It is seen from Figs. 8 and 9 that, while profiles of $\tilde{n}_\xi$, $\tilde{u}_\xi$ and $\tilde{T}_\xi$ of every theory for M=1.1 and M-S and N-S for M=5.0 are almost symmetrical about the origin, the present treatment gives an appreciable asymmetrical profile for M=5.0. Salwen et al[15]. introduced *Asym.* based on the density profile to quantitatively compare the degree of the asymmetry, namely,

$$Asym. = \frac{\{[n(x_G) - n(-\infty)] - [n(\infty) - n(x_G)]\}}{n(\infty) - n(-\infty)}, \tag{51}$$

where x_G refers to the point of maximum-slope of the density profiles.

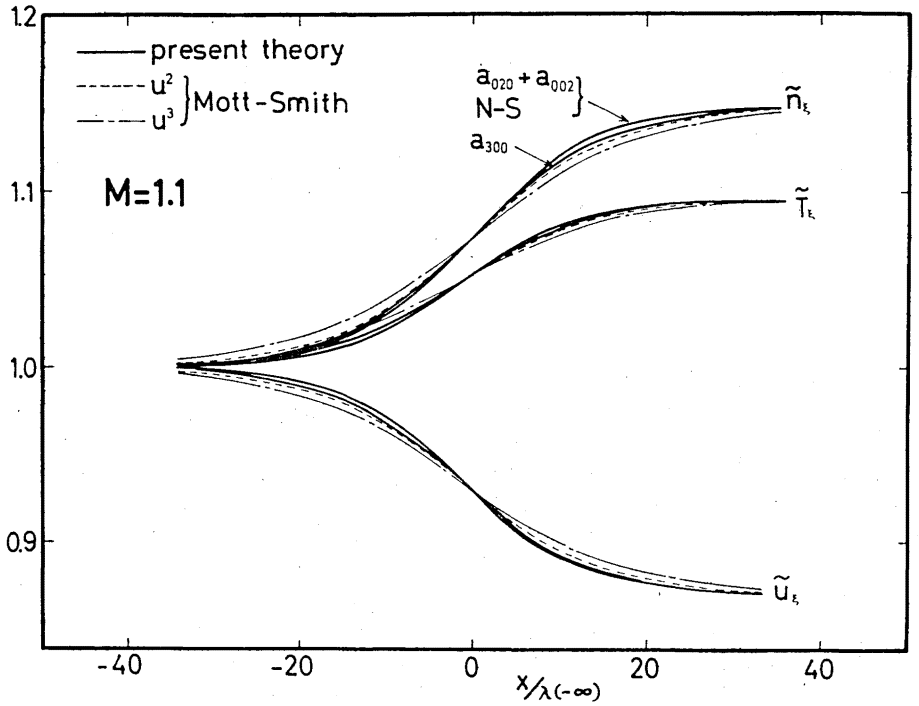

Fig. 8. Profiles of density, velocity and temperature across the shock wave normalized to the respective values at the upstream equilibrium state, M=1.1.

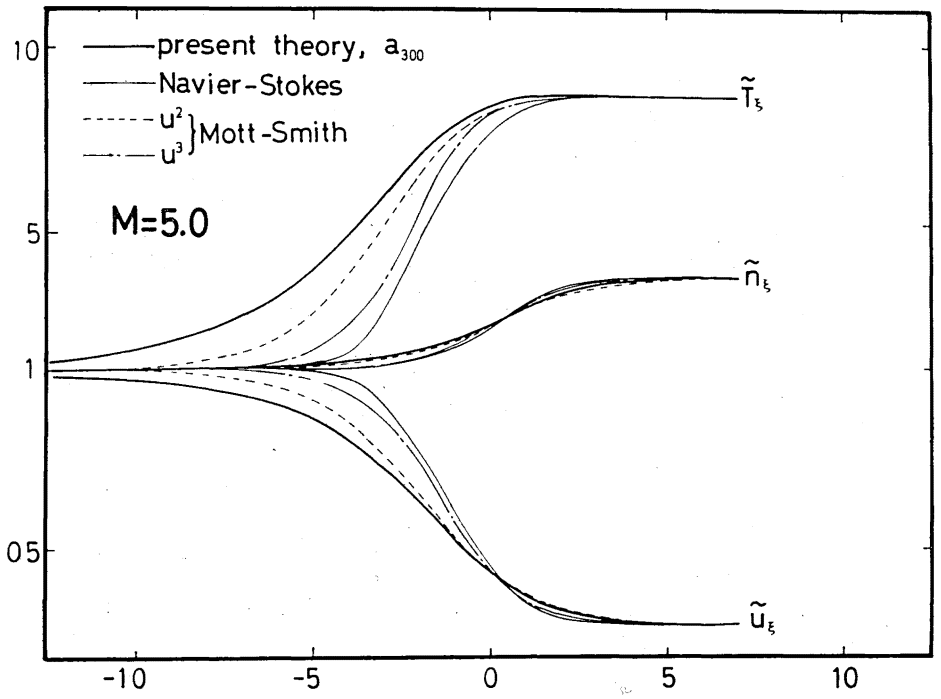

Fig. 9. Profiles of density, velocity and temperature, M=5.0.

The values of the *Asym.* for M=10 are as follows;

	Salwen et al.	Liepmann et al.[20]	present result $a_{300}(x)$
Asym.	3.5%	~20%	5.3%

While the profiles of $\tilde{n}_\xi$, $\tilde{u}_\xi$, and $\tilde{T}_\xi$ have the maximum-slopes at the origin for M=1.1, the maximum-slope points of $\tilde{T}_\xi$ precede those of $\tilde{n}_\xi$ for M=5.0, which is outstanding for the present result.

As there have not yet been done the detailed studies about these points, we cannot know how these effects would actually occur in the real situations. Therefore, further experimental studies about the density profiles (not only the maximum-slope thickness) and the positions of the density and the temperature profiles at high Mach numbers are deeply desired.

The present theory gives the results that the temperature within the shock front becomes greater than that of the downstream equilibrium value for M≥3, (temperature overshoot), the effects which have been already found and discussed by Salwen et al.[15] and Holway[16][17]. This effects will be discussed in some details in Section **VI**.

V. Thermodynamic Considerations

A. At Low Mach Numbers

As has been mentioned, the N-S approximation gives good descriptions to the phenomena for low Mach numbers. The most characteristic feature of this N-S approximation is that the dissipation mechanisms are taken to be linear, namely, that the local stress is proportional to the velocity gradient and the local heat flux to the temperature gradient. Then, the apparent, non-dimensional shear viscosity $\tilde{\mu}$ and heat conductivity $\tilde{\lambda}$ are introduced by calculating the macroscopic variables by the distribution function f, as follows;

$$\tilde{\mu}=\frac{-3\tilde{\sigma}/4}{d\tilde{u}_\xi/d\tilde{\xi}}\ , \tag{52}$$

$$\tilde{\lambda}=\frac{-\tilde{q}_\xi}{d\tilde{T}/d\tilde{\xi}}\ , \tag{53}$$

where $d\tilde{u}_\xi/d\tilde{\xi}$, $d\tilde{T}/d\tilde{\xi}$ are calculated by the equations like Eq. (49), and $\tilde{q}_\xi$ is obtainable from Eq. (46) or (48). $\tilde{T}$ instead of $\tilde{T}_\xi$ has been used in Eq. (53) for the convenience of the comparisons of the treatment with the N-S approximation.

The relation of Eq. (52) is introduced between the lateral stress and the velocity gradient as follows. The pressure tensor, defined by Eq. (40), becomes the diagonal matrix, and among the components of the velocity gradient tensor $\frac{d\mathbf{c}_0}{d\mathbf{r}}+\overline{\frac{d\mathbf{c}_0}{d\mathbf{r}}}$ (where $\overline{\ }$ denotes the conjugate tensor), only $2du_0/dx$ given by Eq. (49) does not vanish, for the assumption of the distribution function of the present theory and M-S. Then the phenomenological linear relation of defining μ

$$\mathbf{P}=-\mu\left(\frac{d\mathbf{c}_0}{d\mathbf{r}}+\overline{\frac{d\mathbf{c}_0}{d\mathbf{r}}}\right)+\frac{2}{3}\mu(\nabla\cdot\mathbf{c}_0)\mathbf{I}+p\mathbf{I}, \tag{54}$$

becomes

$$\sigma_x'=\frac{4}{3}\mu\frac{du_0}{dx},\quad \sigma_y'=\sigma_z'=-\frac{2}{3}\mu\frac{du_0}{dx}, \tag{55}$$

where $\mathbf{I}$ is the unit tensor, p the static pressure

$$p=\frac{1}{3}(p_{xx}+p_{yy}+p_{zz})=n(x)RT(x), \tag{56}$$

and we put

$$\left.\begin{aligned} p_{xx}-p&=-\sigma_x',\\ p_{yy}-p&=-\sigma_y',\\ p_{zz}-p&=-\sigma_z'. \end{aligned}\right\} \tag{57}$$

By calculating Eq. (40), one obtains,

$$\sigma_x' = -\frac{2}{3}m\Big[b_0(u_u-u_0)^2+a_0(u_d-u_0)^2+a_1 2v_d(u_d-u_0) + a_{200}v_d^2-\frac{1}{2}(a_{020}+a_{002})v_d^2\Big], \tag{58}$$

$$\sigma_y' = \sigma_z' = \frac{1}{3}m\Big[b_0(u_u-u_0)^2+a_0(u_d-u_0)^2+a_1 2v_d(u_d-u_0) + a_{200}v_d^2-\frac{1}{2}(a_{020}+a_{002})v_d^2\Big]. \tag{59}$$

σ_x' for the M-S treatment will be obtained by putting $a_1(x)=a_{200}(x)=a_{020}(x)+a_{002}(x)=0$ in Eq. (58). For the present treatment, the values of σ_x' become different by which of $a_{020}(x)+a_{002}(x)$ or $a_{300}(x)$ is retained in the formulation, then the results are shown for each case expressed only by $a_0(x)$ and $b_0(x)$ using Eqs. (18) and (25) or Eqs. (18) and (26), respectively, and non-dimensionalized by using Eqs. (23) and (31) as follows;

(i) M-S:

$$-\tilde{\sigma} = \frac{\sigma_x'}{mb_0(-\infty)u_u^2} = \frac{2}{3}\frac{\beta_0\alpha_0}{\varepsilon\tilde{n}_\xi}(1-\varepsilon)^2, \tag{60}$$

(ii) $a_{020}(x)+a_{002}(x)$:

$$-\tilde{\sigma} = \frac{2}{3}\Big[\frac{\beta_0\alpha_0}{\varepsilon\tilde{n}_\xi}(1-\varepsilon)^2+2(1-\tilde{u}_\xi)(1-\alpha_0-\beta_0)\Big], \tag{61}$$

(ii) $a_{300}(x)$:

$$-\tilde{\sigma} = \frac{2}{3}\Big[\frac{\beta_0\alpha_0}{\varepsilon\tilde{n}_\xi}(1-\varepsilon)^2+\Big\{\frac{4}{5}(1+\varepsilon)-2\tilde{u}_\xi\Big\}(1-\alpha_0-\beta_0)\Big]. \tag{62}$$

Equation (52) is obtained by non-dimensionalizing μ thereby using Eq. (55).

On the other hand, μ and λ of the N-S formulation for the Maxwell molecules ($F=K/r^5$) are given as follows[31];

$$\mu = \frac{5}{8}\frac{\Big(\frac{kmT}{\pi}\Big)^{1/2}\Big(\frac{2kT}{K}\Big)^{1/2}}{A_2\Gamma\Big(\frac{7}{2}\Big)}, \tag{63}$$

$$\lambda = \frac{5}{2}\mu c_v = \frac{75k}{32m}\frac{\Big(\frac{kmT}{\pi}\Big)^{1/2}\Big(\frac{2kT}{K}\Big)^{1/2}}{A_2\Gamma\Big(\frac{7}{2}\Big)}, \tag{64}$$

where $A_2=0.436$, k the Boltzmann constant ($k/m=R$), m the mass of the molecule, and c_v the specific heat at constant volume. By the definitions of $\tilde{\mu}$ and $\tilde{\lambda}$ in Eqs. (52) and (53), respectively,

$$\tilde{\mu}=\frac{\mu}{mb_0(-\infty)u_u l_a}=\frac{2}{3A_2}\tilde{T}=1.53\tilde{T}, \tag{65}$$

$$\tilde{\lambda}=\frac{2}{kl_a b_0(-\infty)u_u}\lambda=\frac{5}{A_2}\tilde{T}=11.5\tilde{T}. \tag{66}$$

Namely, $\tilde{\mu}$ and $\tilde{\lambda}$ of the N-S formulation have the linear relationship with $\tilde{T}$ defined by Eq. (45) or (47). These relations are shown in Fig. 10.

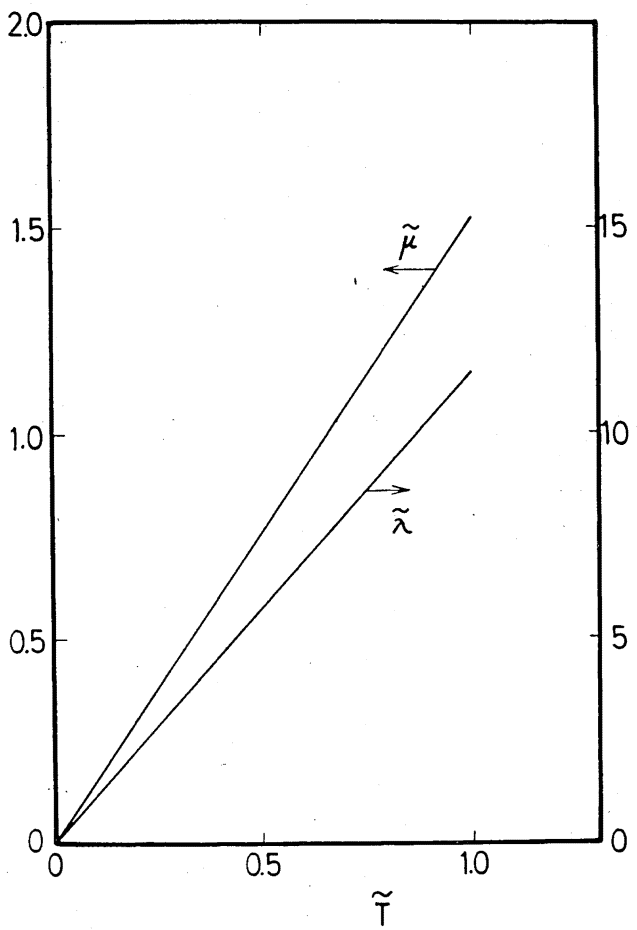

Fig. 10. Temperature dependencies of the viscosity coefficient $\tilde{\mu}$ and thermal conductivity $\tilde{\lambda}$ in the Navier-Stokes approximation.

Each value of the right-hand side of Eqs. (52) and (53) has been calculated for M-S(u^2), M-S(u^3) and for the present treatments, and shown in Figs. 11~14. Figs. 11 and 12 are for M=1.1 and Figs. 13 and 14 for M=1.5. Further, in Figs. 11 and 13 are taken $d\tilde{u}_\xi/d\xi$ for the abscissas and $-3\tilde{\sigma}/4$

for the ordinates, then the gradients at each point give $\tilde{\mu}$ from Eq. (52), and in Figs. 12 and 14 are taken $d\tilde{T}/d\tilde{\xi}$ for the abscissas and $-\tilde{q}_{\xi}$ for the ordinates and the gradients give $\tilde{\lambda}$ from Eq. (53).

In Figs. 11∼14 are also shown $\tilde{\mu}$ and $\tilde{\lambda}$ of the N-S approximation at the up- and down-stream equilibrium corresponding to each temperature by the straight lines which are obtained from Eqs. (65) and (66) or Fig. 10. The lines labelled 'up' correspond to the values for the upstream temperature, and 'down' for the downstream, and the intermediate gradients may be taken within the shock front.

The every curve in Figs. 11∼14 loops from right-bottom to left-top as one proceeds from the upstream to the downstream of the shock wave, then the temperature dependencies of $\tilde{\mu}$ and $\tilde{\lambda}$ for these treatment are almost the same as those for N-S approximation.

It is seen from Fig. 11 that all except for M-S(u^3) have the same tendency and coincide with $\tilde{\mu}$ at the down-stream but have slightly small values at the up-stream than N-S approximation. From Fig. 12, the result for $a_{020}(x)+a_{002}(x)$ is seen to almost coincide with that of N-S, while $a_{300}(x)$ gives too small value and M-S(u^2) and M-S(u^3) too large. It is expected that the N-S approximation gives good descriptions to the phenomena for M= 1.1 and the result for $a_{020}(x)+a_{002}(x)$ is near to the N-S formulation, then

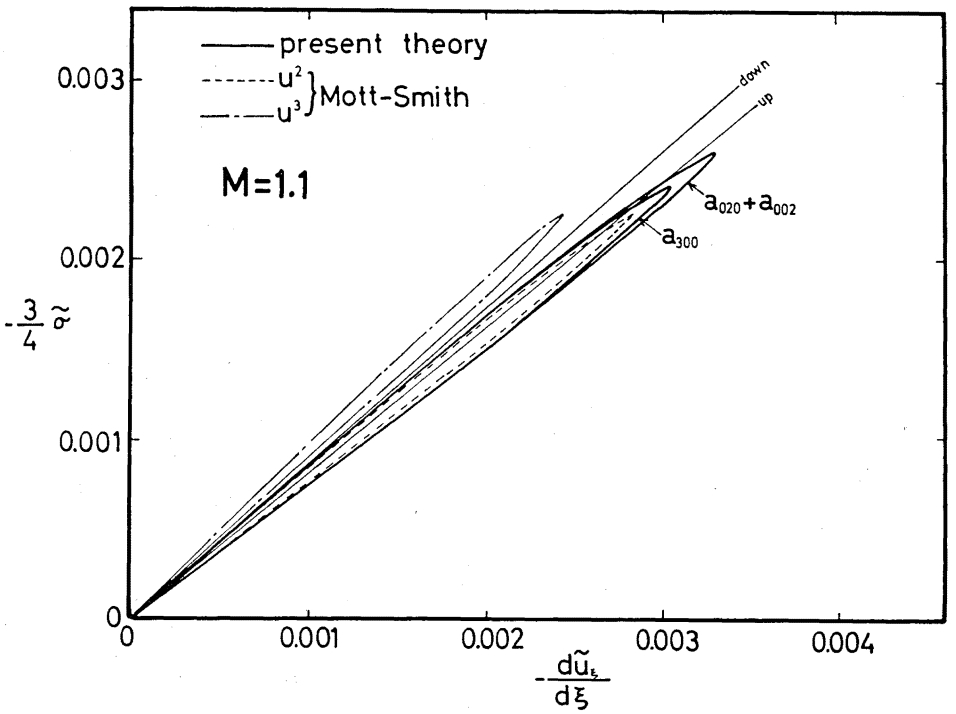

Fig. 11. Viscosity, M=1.1.

we can readily expect that $a_{020}(x)+a_{002}(x)$ would gives reasonable result for these low Mach number range and this has been partly verified by the density profiles in Figs. 4 and 6. Further, it can be said that the differences in the density profiles of M-S(u^2) and $a_{300}(x)$ (Figs. 4 and 6) from N-S approximation are due to the poor descriptions of the heat flux shown in Fig. 12 and that M-S(u^3) does not properly express both the viscosity and heat flux.

$\tilde{\mu}$ and $\tilde{\lambda}$ shown in Figs. 13 and 14 for M=1.5 are larger for the present treatments than those of the N-S approximation but still nearer to N-S than, M-S.

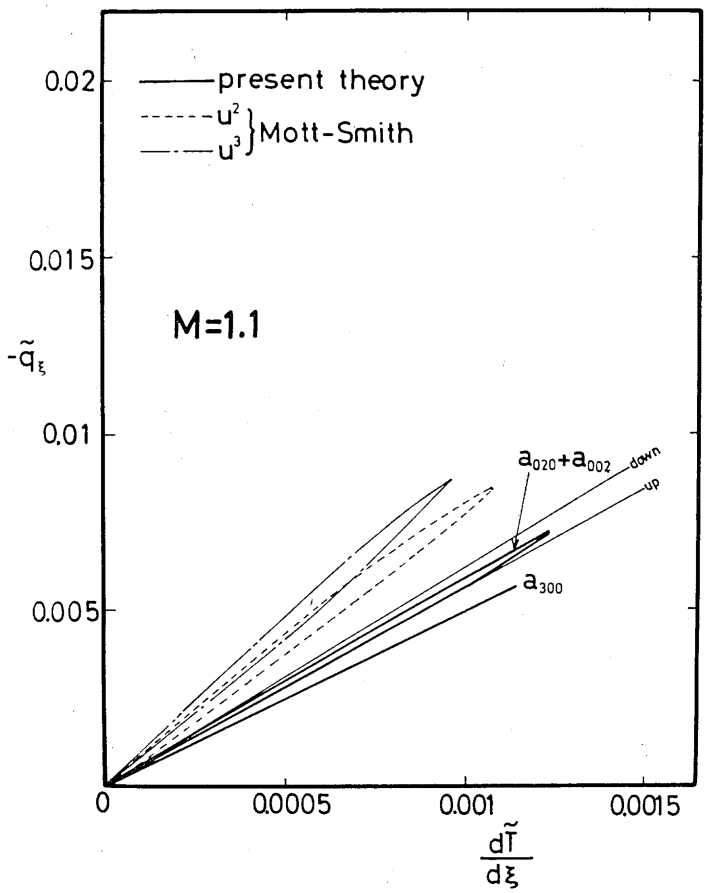

Fig. 12. Thermal conductivity, M=1.1.

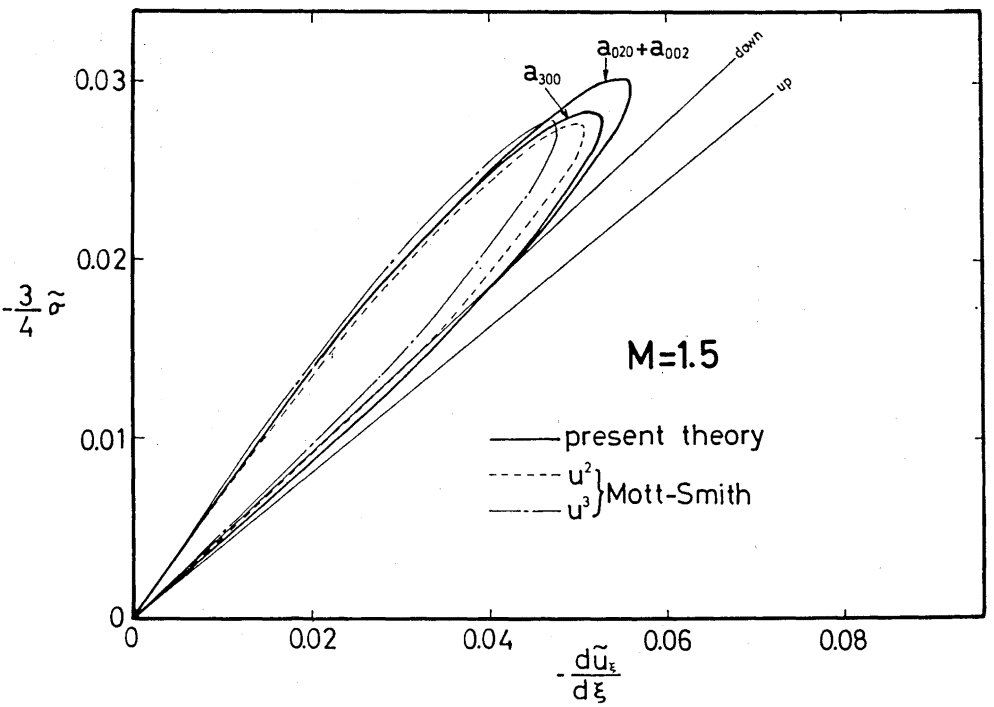

Fig. 13. Viscosity, M=1.5.

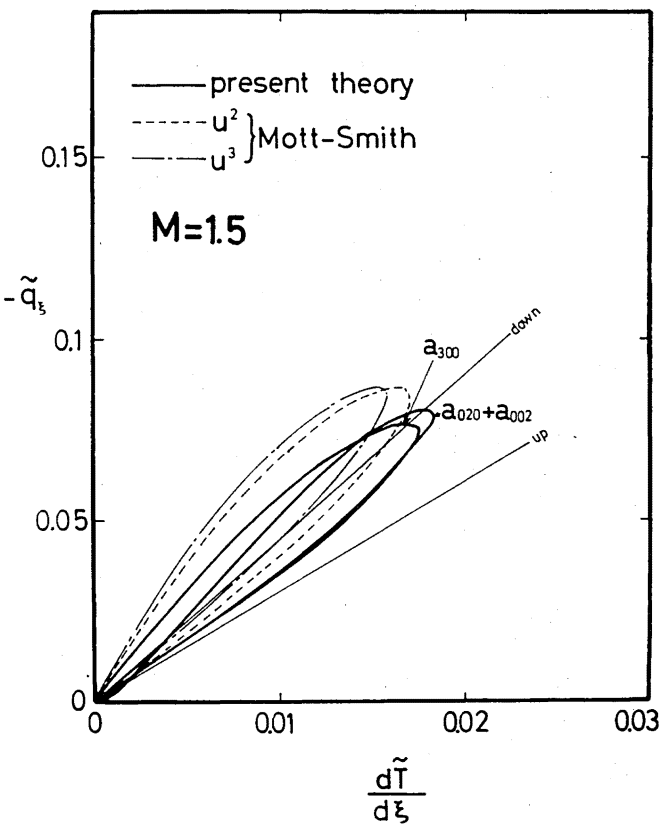

Fig. 14. Thermal conductivity, M=1.5.

B. At High Mach Numbers

There is no standard of comparison for higher Mach numbers, like N-S approximation for low Mach numbers, and as has been already mentioned, only the experimental density profiles (mainly the maximum-slope shock thickness) have been found to be properly described by M-S(u^2). Consequently, after being proposed a new theory of the shock structure, it has become a usual way to compare the theoretical shock thicknesses with those of M-S(u^2). But, as the detailed non-equilibrium state in the shock front are not wholly described only by the density profiles, further considerations are needed in order to get clearer insight into the phenomena and this will be discussed in some details in the next section.

In order to compare the present treatments and M-S with the linear dissipation theory (N-S approximation), $\tilde{\mu}$ and $\tilde{\lambda}$ defined in **A** are shown in Figs. 15 and 16 for M=5.0. It is seen from these figures that the results of M-S and $a_{300}(x)$ give larger values of $\tilde{\mu}$ and $\tilde{\lambda}$ and, further, the roundings at the right-side become appreciable. These latter effects correspond to the facts that the maximum points of the velocity and temperature gradients do not coincide with those of the lateral stress and heat flux, and these do not appear in the formulation based on the linear dissipation.

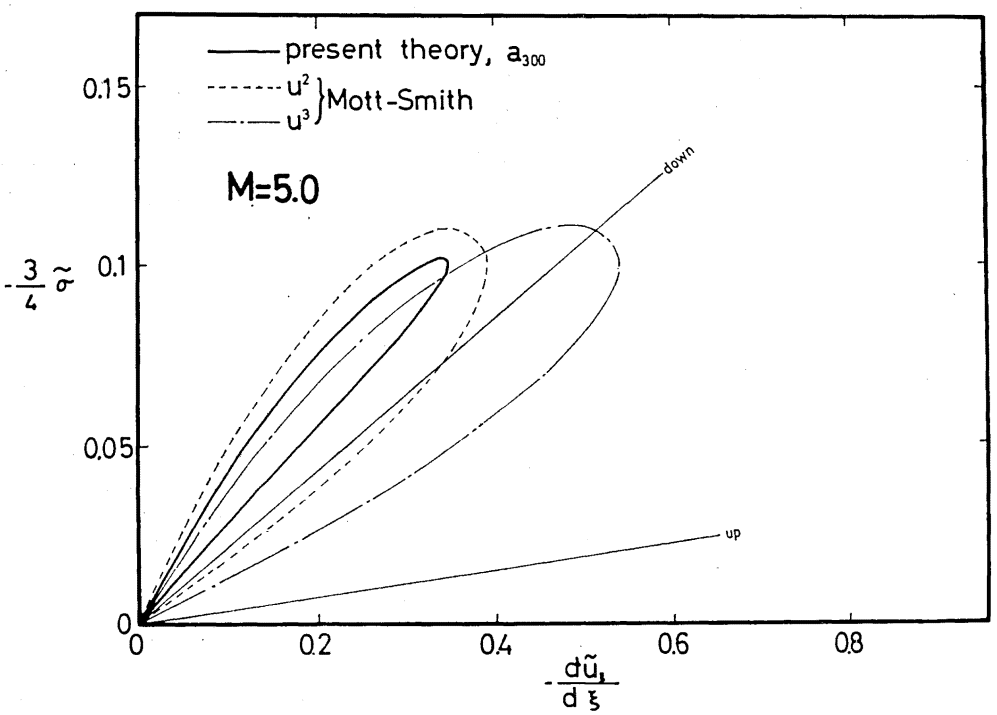

Fig. 15 Viscosity, M=5.0.

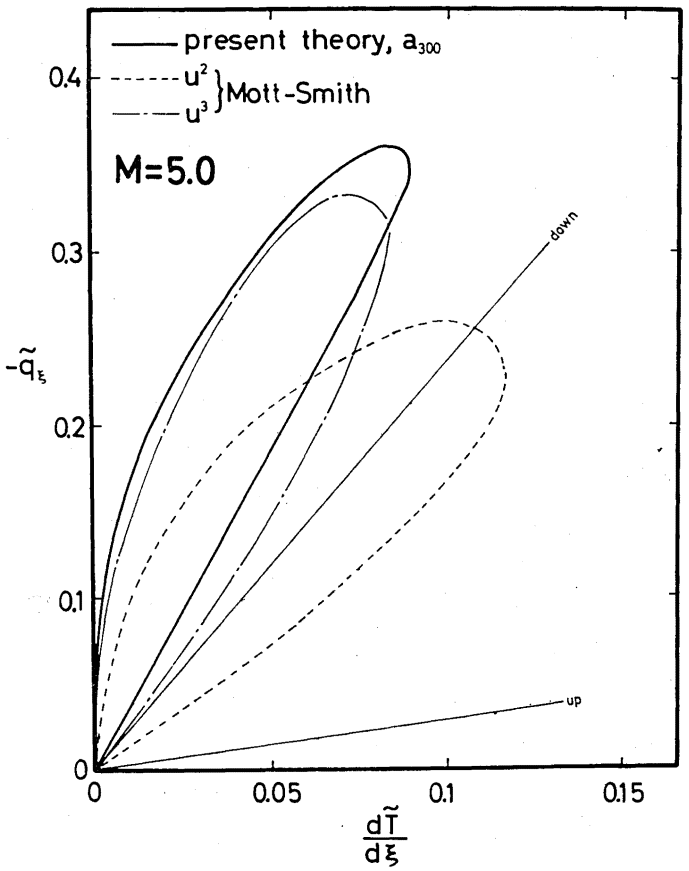

Fig. 16. Thermal conductivity, M=5.0.

There is portion in Fig. 16 where the temperature gradient takes the negative values and it is the consequence of the temperature overshoot referred to in Section **IV-B.**

VI. Discussion

Energy dissipation mechanisms determine the shock wave structure. Density, velocity and temperature may change stepwise for the case of no dissipation, but in reality, the dissipative forces act to flatten these steep gradients and the steady shock front is maintained at the balanced states between these actions. When the Mach number is small and the shock wave seems to be near to the sound wave, the gradients of the temperature and velocity are small, then the heat flux and the lateral stress may be treated as proportional to, respectively, the temperature and velocity gradients. The formulation based on this idea is the N-S approximation and the results

obtained from this formulation give the reasonable results for $1 \leq M \leq 1.5$ judging from the comparison of the results with the experimental observations. While, as the Mach numbers become larger, the gradients of temperature and velocity become steeper and the formulations based on the linear dissipations insufficient. Furthermore, the velocity distribution function may be appreciably skewed from the Gaussian, then the temperature, for example, may lose its meaning as the state variable at the thermodynamic equilibrium, if one artificially extends the definition of the temperature as the average of the kinetic energy of particles in the velocity space. Mott-Smith[3] overcame these difficult situations by resorting to the kinetic theoretical viewpoint rather than the thermodynamic one, but his method gives the results which differ from the phenomena at low Mach numbers, and further there is no justification that the other thermodynamic variables than density may be described by his method. No detailed, quantitative discussion has been done on these points so far. While the present method may be thought of as the extension of the M-S method, it gives reasonable results for both of low and high Mach number ranges.

The macroscopic thermodynamic variable $<Q>$ is given as the mean value of the dynamic variable $Q(\mathbf{c})$ as follows:

$$<Q> = \frac{1}{n(x)} \int Q(\mathbf{c}) f(x, \mathbf{c}) d\mathbf{c}. \tag{67}$$

Substituting expansion Eq. (11) into this form and calculating some moments of low order, one obtains Table 1 in which the thermodynamic meaning of each moment and the coefficients which remain in $<Q>$ are given, (cf. Sec. **IV**). Here, as the average velocities in the y and z directions are zero, $a_{010}(x) = a_{001}(x) = 0$ are obtained, which were used in Eq. (15) to get $a_{110}(x) = a_{101}(x) = 0$.

Table. 1.

$<Q>$	thermodynamic meaning	coefficients that are retained in $<Q>$
$<1> = n(x)$	particle density	b_0, a_0
$<v> = u_0(x) n(x)$	average velocity in x direction	b_0, a_0, a_1
$<v> = 0$	average velocity in y direction	$a_{010} = 0$
$<w> = 0$	average velocity in z direction	$a_{001} = 0$
$<(\mathbf{c}-\mathbf{i}u_0)^2>/3Rn(x)$	temperature	$b_0, a_0, a_1, a_{200}, a_{020}, a_{002}$
$2<(\mathbf{c}-\mathbf{i}u_0)^2(u-u_0)>/m$	heat flux in x direction	$b_0, a_0, a_1, a_{200}, a_{020}, a_{002}, a_{300}$
$2<(\mathbf{c}-\mathbf{i}u_0)^2 v>/m$	heat flux in y direction	0
$2<(\mathbf{c}-\mathbf{i}u_0)^2 w>/m$	heat flux in z direction	0

In the present method, the unknown coefficients of expansion Eq. (11) are determined by substituting Eq. (11) to the moment equations of the Boltzmann equation, Eq. (13). In order to make the formulation within the finite numbers of moment equations, Eq. (11) should be truncated at some

proper terms. The different results are obtained for each method of truncation (M-S treatment may be seen as the O-th approximation of the present treatment), the physical meaning of the choices of terms should be clarified by referring to the considerations based on Table 1, etc.

While in the present method, five conservation equations are made independent (Eqs. (14)$\sim$(16)) and the two moment equations for $\Phi(\mathbf{c})=u^2$ and u^3 (Eqs. (27) and (28) or (29) and (30)) are used, it can be shown that the moment equations for $\Phi(\mathbf{c})=v^2, v^3, w^2, w^3$, uv and vw are filled in this formulation (cf. Appendix). Consequently, the transport relations for the pressure tensor and heat flow are independently taken into the formulation besides those of the conservation relations for mass, momentum and energy. On the other hand, in the M-S approximation, three conservation equations reduce to the one independent equation, then the characteristics of each mode of transport for mass, momentum and energy cannot be taken into the formulation.

By performing the calculations described above and comparing the obtained results, it turned out that the differences in the distribution function themselves for every method at the fixed location in space are not large, then comparisons should be made for the macroscopic variables which are given by Eq. (67).

As has been frequently mentioned, N-S approximation gives good results for low Mach numbers, the distribution function in this method is skewed from the local equilibrium one to take the moments up to the heat flow into the formulation. By referring to Table 1, it is seen that the formulation of adopting $a_{020}(x)+a_{002}(x)$ is very close to this N-S approximation in that the moments from the lowest order up to the heat flow have been correctly taken into considerations, only the approximation done is the fact that the coefficients higher than $a_{300}(x)$ are neglected in the conservation and u^3 transport equations. Meanwhile, for the case of adopting $a_{300}(x)$, the descriptions are incorrect for the pressure tensor which is a lower moment than the heat flux, but each conservation relation, the pressure tensor and heat flux are independently taken into the formulation. Compared with these treatments, it is obvious that the M-S methods appreciably differ from N-S approximation, especially so for M-S(u^3) in which a lower moment (u^2) is neglected. Based on these considerations, we can see from Figs. 11 and 12 for M=1.1 the following facts: while M-S(u^2), $a_{020}(x)+a_{002}(x)$ and $a_{300}(x)$ give the same order of approximation for the viscosity (Fig. 11), the agreement of the result of $a_{020}(x)+a_{002}(x)$ with N-S approximation is fair for the thermal conductivity, and the results of $a_{300}(x)$ and M-S(u^2) appreciably deviate from this (Fig. 12). On the other hand, M-S(u^3) in which the lower moment is neglected, gives the results which considerably differ both for $\tilde{\mu}$ and $\tilde{\lambda}$ from the result of N-S.

Meanwhile, the treatments of Salwen et al.[15] and Holway[16][17] give the results which almost coincide with that of N-S. In the former method, one more Gaussian distribution function is superposed to the bimodal distribution function of M-S, then five conservation equations are made independent, and

two moment equations of u^2 and u^3 or u^2 and $u(u^2+v^2+w^2)$ are employed to determine seven unknowns. The degree of the proximity of this method to the N-S formulation at low Mach numbers seems to be the same order with that of $a_{020}(x)+a_{002}(x)$ of the present method, in that the heat flow was taken into consideration as a small skewing of the distribution function from the equilibrium one. In the latter, Holway made five conservation equations independent by increasing variables from those of M-S by making the distinction of the temperature in the x and y-z directions and used seven moment equations from the lowest order, as was done by the present author and Salwen et al., and in this respect this method is seen to be improved from that of M-S at low Mach numbers.

From these considerations, the thermodynamic contents of the methods which are recently proposed as to improve the M-S method at low Mach number become clear. Furthermore, it is easily known that the 'two fluid model' method of Ziering et al.[19] has improved that of M-S (in spite of the same form of the distribution functions for both cases) because they increased independent variables by introducing transition probabilities of various modes and could make the conservation equations independent. In this respect, it can be said that they could find the, so to say, *hidden variables* in the different method from those of the present author, Salwen et al. and Holway.

At higher Mach numbers, it is expected that the contributions from higher moments will become important and the present method to adopt $a_{020}(x)+a_{002}(x)$ would not be possible to describe the phenomena in this high Mach regions. Actually, there is no solution for $M \geq 2.05$. (The same situations are found in the methods of, for example, Grad[4].) Similarly, in the method of Salwen et al., the contributions to the heat flow are determined by the positions and heights of the three Gaussians in the velocity space, and the character proper to the heat flow may not be taken into the formulation. The methods of Holway and 'two-fluid model' method would be in the similar situation and it is thought that each of these will become to a poor description to the phenomena at high Mach numbers.

On the other hand, the present method of adopting $a_{300}(x)$ is not a correct description in that the viscosity, which is the lower moment than heat flux, is not correctly taken into the formulation (and this effect plays an important role at low Mach numbers, cf. Figs. 11 and 12), but the term characteristic of the heat flow, $a_{300}(x)$, are considered and this method is expected to give good descriptions of the phenomena at high Mach numbers. The experimental measurements are performed only on the density profile across the shock front so far, and it is admitted that M-S (u^2) can reproduce these experimental values properly and the result of $a_{300}(x)$ gives almost the same order of approximation to the density profiles, while the various methods cited above give fairly different results.

By the way, the reason why M-S(u^2) can give the plausible result in the density profile is thought to be due to the fact that the term, which is proper to the heat flow and is neglected in this formulation, may counterbalance the contri-

butions from higher moments as to the effects on the density profile. This fact is expected from the followings: in the heat flow, M-S(u^3) gives rather similar result to that of $a_{300}(x)$ at high Mach numbers (cf. Fig. 14) than that of M-S(u^2), and the distribution function of M-S itself appreciably deviates from that of $a_{300}(x)$ (cf. Fig. 3), and in spite of these facts, the density profiles for M-S(u^2) are almost the same as those of $a_{300}(x)$ (cf. Fig. 4 and 6). Consequently, the higher moments of the distribution function than density, temperature for instance, are expected to become different from the results obtained from M-S(u^2) (cf. Fig. 9) or more generally, the true distribution function may be different from that obtained by M-S(u^2) but there is, so far, no experimental confirmation on these points.

In the meanwhile, temperature overshoot is found for $M \geq 3$, similar to the results of Salwen et al.[15] and Holway[16)17)]. There is no change in sign of heat flux at this temperature maximum point, then this effect is impossible from the usual relations between heat flow and temperature gradient. This fact suggests that the usual meaning of temperature has been lost at this high degree of deviation from equilibrium when it is formally defined by Eq. (39), or that higher terms than $a_{300}(x)$ should be retained in the formulation at this high Mach numbers. (For the latter, the effect of truncation may reflect on the temperature, though the terms only up to $a_{020}(x)$, $a_{002}(x)$ are retained in $T(x)$, cf. Eq. (39) and Table 1. This similar effect was found for the density $n(x)$ in which the terms of only $b_0(x)$ and $a_0(x)$ are retained in $n(x)$ but the present treatment gives better results than those of M-S.). While there is a proof[22)] that no temperatune overshoot is found for monatomic gas in the M-S bimodal distribution function method, this does,not necessarily show that the M-S method gives good descriptions of the phenomena.

VII. Conclusion

The problem of the steady, one-dimensional shock wave structure of monatomic single component gas has been treated by expanding the velocity distribution function of Boltzmann equation by Eq. (11), and the thermodynamic variables within the shock front calculated. As the results, it becomes clear why the various theoretical methods could be brought to the closer approximations to the N-S method than M-S at low Mach numbers and that the contributions from the higher moments become important for high Mach numbers but the density profiles could be properly expressed by M-S(u^2).

While there could be various other methods to this problem, it is thought that qualitatively unified explanations could have been gained by the present treatment. At higher Mach numbers $M > 10$, the excitations of the internal degrees of freedom (excitations of the trapped electron energy levels from the ground state and ionization etc.) would become important, and for this case the treatment from the different aspects would become necessary.

The numerical calculations of this work have been performed by the OKITAC-5090 H of the Computation Center of Kyushu University.

Acknowledgment

The author would like to express his sincere gratitude to Professors T. Ikui and T. Murakami for their continual suggestions and encouragements during the course of this work.

References

1) R. Becker, Z. Physik 8, 321(1921-1922).
2) D. Gilbarg and D. Paolucci, J. Ratl. Mech. Anal. 2, 617(1953).
3) H. M. Mott-Smith, Phys. Rev. 82, 885(1951).
4) H. Grad, Commun. Pure Appl. Math. 5, 257(1952).
5) F. S. Sherman, NACA TN 3298(1955).
6) L. Talbot and F. S. Sherman, NASA Memo 12-14-58W (1959).
7) K. Hansen and D. F. Hornig, J. Chem. Phys. 33, 913(1960).
8) M. Linzer and D. F. Hornig, Phys. Fluids 6, 1661(1963).
9) M. Camac, in *Rarefied Gas Dynamics*, J. H. de Leeuw, Ed. (Academic Press, Inc., New York, 1965), vol. 1, p. 240.
10) F. Robben and L. Talbot, Phys. Fluids 9, 633(1966).
11) P. V. Marrone, Phys. Fluids 10, 521(1967).
12) L. Talbot, ARS J. 32, 1009(1962).
13) S. Chapman and T. G. Cowling, *The Mathematical Theory of Non-Uniform Gases*, (Cambridge University Press, London, 1952).
14) L. M. Schwartz and D. F. Hornig, Phys. Fluids 6, 1669(1963).
15) H. Salwen, C. E. Grosch, and S. Ziering, Phys. Fluids 7, 180(1964).
16) L. H. Holway Jr., in *Rarefied Gas Dynamics*, J. H. de Leeuw, Ed. (Academic Press, Inc., New York, 1965), vol. 1, p. 193.
17) L. H. Holway Jr., in *Rarefied Gas Dynamics*, C. L. Brundin, Ed. (Academic Press, Inc., New York, 1967), vol. 1, p. 759.
18) S. H. Radin and D. Mintzer, Phys. Fluids 9, 1621(1966).
19) S. Ziering, F. Ek, and P. Koch, Phys. Fluids 4, 975(1961).
20) H. W. Liepmann, R. Narashimha, and M. T. Chahine, Phys. Fluids 5, 1313(1962).
21) M. T. Chahine and R. Narashimha, in *Rarefied Gas Dynamics*, J. H. de Leeuw, Ed. (Academic Press, Inc., New York, 1965), vol. 1, p. 140.
22) W. A. Gustafson, Phys. Fluids 3, 732(1960).
23) K. Muraoka and T. Ikui, Phys. Fluids 11, 1129(1968).
24) M. M. Oberai, Phys. Fluids 8, 826(1965).

(Received October 25, 1968)

Appendix

The Collison Moments for the Maxwell Molecules

It is often necessary to calculate the moments of the Boltzmann equation for some dynamical variables, not only in the case of the calculations of the shock wave structure problem shown in the text and elsewhere[23], but for other problems like those in rarefied gas dynamics. Then, it would be of value to summarize some lower moments for the Boltzmann collision term for the case of the Maxwell molecules (interparticle force $F=K/r^5$), in order to eliminate the undue duplications of the same calculation procedures.

A1. Dynamics of collision

Fig. A·1 shows the relative coordinate system of binary collision among the particles of mass m_1 and m_2, m_1 being fixed in space, χ the deflection angle, and $\mathbf{j}$ the unit vector along the apse-line of the passage of the particle

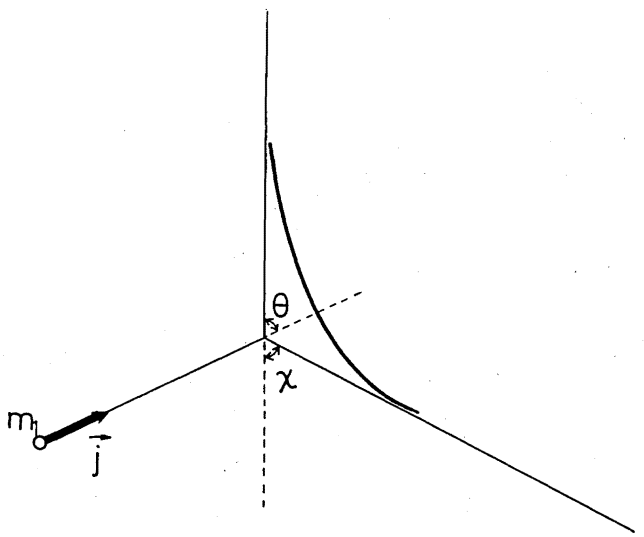

Fig. A·1. Trajectory of molecule m_2 relative to molecule m_1.

m_2. Then, (cf. Ref. 13),

$$\mathbf{c}_1'-\mathbf{c}_1=\frac{2m_2}{m_1+m_2}g\cos\theta\cdot\mathbf{j} \tag{A·1}$$

where $\mathbf{c}$ is the velocity of particle, g the initial relative velocity, the primed quantities represent the values after the collision, and suffix 1 shows the value for particle m_1. Then, by referring to the notations in Fig. A·2, we obtain

$$\mathbf{i}_x\cdot\mathbf{j}=\cos\zeta_x=\cos\theta\cos\psi_x+\sin\theta\sin\psi_x\cos\phi_x \tag{A·2}$$

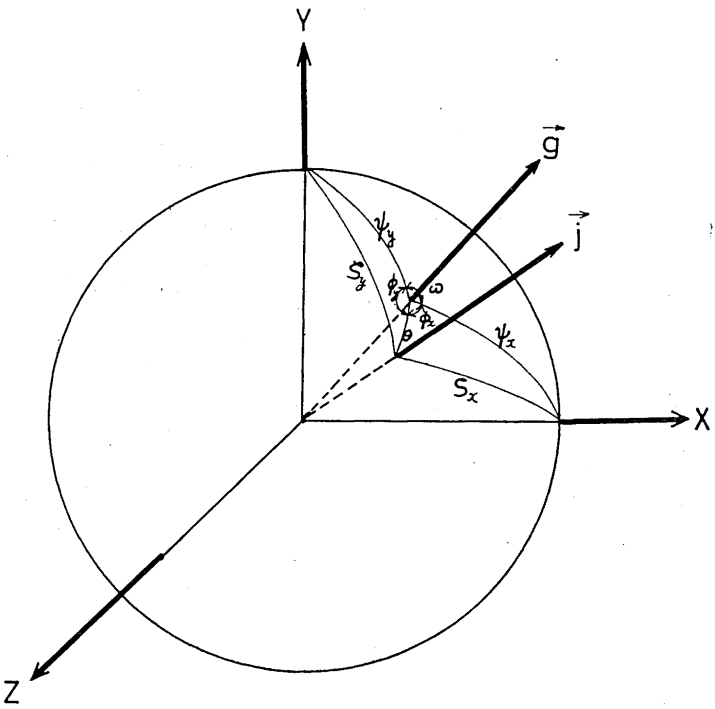

Fig. A·2 Spatial orientations of vectors **g** and **j**.

$$\mathbf{i}_y\cdot\mathbf{j}=\cos\zeta_y=\cos\theta\cos\psi_y+\sin\theta\sin\psi_y\cos\phi_y$$
$$=\cos\theta\cos\psi_y+\sin\theta\sin\psi_y(\cos\phi_x\cos\omega-\sin\phi_x\sin\omega) \qquad (A\cdot3)$$

where $\mathbf{i}_x$ and $\mathbf{i}_y$ are the unit vectors along x and y axis, respectively, and use was made the following relations to obtain the last expressions in Eq. (A. 3):

$$\cos\frac{\pi}{2}=\cos\psi_x\cos\psi_y+\sin\psi_x\sin\psi_y\cos\omega$$
$$\therefore\ \cos\omega=-\frac{\cos\psi_x\cos\psi_y}{\sin\psi_x\sin\psi_y}\ , \qquad (A\cdot4)$$
$$\phi_y=2\pi-\phi_x-\omega. \qquad (A\cdot5)$$

And further, the following relations are obtainable;

$$\cos\psi_x=\frac{u_2-u_1}{g},\qquad \cos\psi_y=\frac{v_2-v_1}{g} \qquad (A\cdot6)$$
$$\chi=\pi-2\theta. \qquad (A\cdot7)$$

A2. Transport equation for $\Phi(\mathbf{c})$

The Boltzmann equation for the binary mixture may be written as follows[13]:

$$Df_1=\frac{\partial f_1}{\partial t}+\mathbf{c}_1\cdot\frac{\partial f_1}{\partial \mathbf{r}}+\mathbf{F}\cdot\frac{\partial f_1}{\partial \mathbf{c}_1}=\left(\frac{\partial f_1}{\partial t}\right)_{coll}$$

$$=\iiint(f_1'f'-f_1f)\,gbdbd\phi_x d\mathbf{c}+\iiint(f_1'f_2'-f_1f_2)\,gbdbd\phi_x d\mathbf{c}_2, \qquad (A\cdot8)$$

where $\mathbf{r}=(x, y, z)$, $\mathbf{c}=(u, v, w)$, $\mathbf{F}$ is the force acting on the unit mass, and b is the impact parameter. The moment or transport equation for an arbitrary dynamical variable $\Phi(\mathbf{c})$ is written as,

$$\int Df_1\Phi(\mathbf{c}_1)d\mathbf{c}_1=\int\left(\frac{\partial f_1}{\partial t}\right)_{coll}\Phi(\mathbf{c}_1)\,d\mathbf{c}_1$$

$$=\iiiint(f_1'f'-f_1f)\,\Phi(\mathbf{c}_1)\,gbdbd\phi_x d\mathbf{c}d\mathbf{c}_1+\iiiint(f_1'f_2'-f_1f_2)\,\Phi(\mathbf{c}_1)\,gbdbd\phi_x d\mathbf{c}_1d\mathbf{c}_2$$

$$=\iiiint\{\Phi(\mathbf{c}_1')-\Phi(\mathbf{c}_1)\}f_1f\,gbdbd\phi_x d\mathbf{c}d\mathbf{c}_1+\iiiint\{\Phi(\mathbf{c}_1')-\Phi(\mathbf{c}_1)\}f_1f_2gbdbd\phi_x d\mathbf{c}_1d\mathbf{c}_2$$

$$\equiv\triangle_{11}\Phi(\mathbf{c})+\triangle_{12}\Phi(\mathbf{c}). \qquad (A\cdot9)$$

A3. Calculations for some lower moments

In the following the calculations are performed for some lower moments which are of practical importance, and that for $\triangle_{12}\Phi(\mathbf{c})$ in Eq. (A·9). $\triangle_{11}\Phi(\mathbf{c})$ will be easily obtained by merely changing the suffix 2 to 1 in the final results.

(A3-i) $\Phi(\mathbf{c})=u$:

$$u_1'-u_1=(\mathbf{c}_1'-\mathbf{c}_1)_x=\frac{2m_2}{m_1+m_2}g\cos\theta(\mathbf{i}_x\cdot\mathbf{j})$$

$$=\frac{2m_2}{m_1+m_2}g\cos\theta(\cos\theta\cos\psi_x+\sin\theta\sin\psi_x\cos\phi_x). \qquad (A\cdot10)$$

If we put the contributions from the integrals of b and ϕ_x as I_u, and by using the factor of v_0 of Chapman-Cowling notation[13],

$$I_u\equiv\int_{\phi_x=0}^{2\pi}\int_{v_0=0}^{\infty}(u_1'-u_1)\,v_0dv_0d\phi_x$$

$$=2\pi\frac{m_2}{m_1+m_2}A_1(u_2-u_1).$$

$$\therefore\ \triangle_{12}u\cdot\left[\pi\left(\frac{m_1+m_2}{m_1m_2}K_{12}\right)^{1/2}\right]^{-1}=\iint\frac{2m}{1+m}A_1(u_2-u_1)f_1f_2d\mathbf{c}_1d\mathbf{c}_2, \qquad (A\cdot11)$$

where K_{12} is the force constant for the Maxwell molecules, $m=m_2/m_1$, and $A_1=\int_0^{\infty}(1-\cos\chi)\,v_0dv_0=0.422$.

(A-ii) $\Phi(\mathbf{c})=u^2$:

Oberai[24] performed the calculations for this case and obtained

$$\triangle_{12}u^2\cdot\left[\pi\left(\frac{m_1+m_2}{m_1m_2}\right)K_{12}\right]^{1/2}\Big]^{-1}$$

$$=\iint\left\{4A_1\frac{m}{1+m}u_1(u_2-u_1)+(4A_1-2A_2)\left(\frac{m}{1+m}\right)^2(u_2-u_1)^2\right.$$

$$\left.+A_2\left(\frac{m}{1+m}\right)^2\left((v_2-v_1)^2+(w_2-w_1)_2\right)\right\}f_1f_2d\mathbf{c}_1d\mathbf{c}_2 \qquad (A\cdot12)$$

where $A_2=\int_0^\infty(1-\cos^2\chi)v_0dv_0=0.436.$

(A3-iii) $\Phi(\mathbf{c})=u^3$:

By the similar calculation Procedures as for the above two cases, the following results are obtained;

$$\triangle_{12}u^3\cdot\left[\pi\left(\frac{m_1+m_2}{m_1m_2}K_{12}\right)^{1/2}\right]^{-1}$$

$$=\iint\Big[6A_1\frac{m}{1+m}u_1^2(u_2-u_1)$$

$$+12\left(\frac{m}{1+m}\right)^2u_1\left\{(u_2-u_1)^2\left(A_1-\frac{A_2}{2}\right)+\frac{A_2}{4}\left((v_2-v_1)^2+(w_2-w_1)^2\right)\right\}$$

$$+\left(\frac{m}{1+m}\right)^3\left\{3(u_2-u_1)\left((u_2-u_1)^2+(v_2-v_1)^2+(w_2-w_1)^2\right)(A_1+A_2-A_3)\right.$$

$$\left.+(u_2-u_1)^3(3A_1-9A_2+5A_3)\right\}\Big]f_1f_2d\mathbf{c}_1d\mathbf{c}_2, \qquad (A\cdot13)$$

where $A_3=\int_0^\infty(1-\cos^3\chi)v_0dv_0=0.532.$

(A3-iv) $\Phi(\mathbf{c})=v$:

$$v_1'-v_1=(\mathbf{c}_1'-\mathbf{c}_1)_y=\frac{2m_2}{m_1+m_2}g\cos\theta\,(\mathbf{i}_y\cdot\mathbf{j})=\frac{2m_2}{m_1+m_2}g\cos\theta\cos\zeta_y. \qquad (A\cdot14)$$

By the same procedure as to obtain Eq. (A. 11), one gets

$$I_v\equiv\int_{\phi_x=0}^{2\pi}\int_{v_0=0}^{\infty}(v_1'-v_1)v_0dv_0d\phi_x=2\pi\frac{m_2}{m_1+m_2}(v_2-v_1)A_1.$$

$$\therefore\ \triangle_{12}v\cdot\left[\pi\left(\frac{m_1+m_2}{m_1m_2}K_{12}\right)^{1/2}\right]^{-1}=\iint\frac{2m}{1+m}A_1(v_2-v_1)f_1f_2d\mathbf{c}_1d\mathbf{c}_2. \qquad (A\cdot15)$$

(A3-v) $\Phi(\mathbf{c})=v^2$:

$$\triangle_{12}v^2\cdot\left[\pi\left(\frac{m_1+m_2}{m_1m_2}K_{12}\right)^{1/2}\right]^{-1}$$

$$=\iint\Big[\frac{4m}{1+m}v_1(v_2-v_1)A_1$$

$$+\frac{1}{2}\left(\frac{2m}{1+m}\right)^2\left\{2A_1(v_2-v_1)^2+\frac{A_2}{2}\Big((u_2-u_1)^2-2(v_2-v_1)^2+(w_2-w_1)^2\Big)\right\}\Big]f_1f_2d\mathbf{c}_1d\mathbf{c}_2. \tag{A·16}$$

(A3-vi) $\Phi(\mathbf{c})=v^3$:

$$\triangle_{12}v^3\cdot\left[\pi\left(\frac{m_1+m_2}{m_1m_2}K_{12}\right)^{1/2}\right]^{-1}$$

$$=\iint\Big[3A_1\frac{2m}{1+m}v_1^2(v_2-v_1)$$

$$+\frac{3}{2}\left(\frac{2m}{1+m}\right)^2\left\{\frac{A_2}{2}v_1\Big((u_2-u_1)^2-2(v_2-v_1)^2+(w_2-w_1)^2\Big)+2A_1v_1(v_2-v_1)^2\right\}$$

$$+\left(\frac{2m}{1+m}\right)^3\left\{\frac{3A_1-3A_2+A_3}{4}(v_2-v_1)^3\right.$$

$$\left.+\frac{3}{8}(A_1+A_2-A_3)(v_2-v_1)\Big((u_2-u_1)^2+(w_2-w_1)^2\Big)\right\}\Big]f_1f_2d\mathbf{c}_1d\mathbf{c}_2. \tag{A. 17}$$

(A3-vii) $\Phi(\mathbf{c})=uv^2$:

$$\triangle_{12}uv^2\cdot\left[\pi\left(\frac{m_1+m_2}{m_1m_2}K_{12}\right)^{1/2}\right]^{-1}$$

$$=\iint\Big[\frac{2m}{1+m}A_1\Big\{2u_1v_1(v_2-v_1)+v_1^2(u_2-u_1)\Big\}$$

$$+\left(\frac{2m}{1+m}\right)^2\left\{A_1u_1(v_2-v_1)^2+\frac{A_2}{4}u_1\Big((u_2-u_1)^2-2(v_2-v_1)^2+(w_2-w_1)^2\Big)\right.$$

$$\left.+(2A_1-\frac{3}{2}A_2)v_1(u_2-u_1)(v_2-v_1)\right\}$$

$$+\left(\frac{2m}{1+m}\right)^3\left\{\frac{A_1-2A_2+A_3}{2}(u_2-u_1)(v_2-v_1)^2\right.$$

$$\left.+\frac{A_1+A_2-A_3}{8}(u_2-u_1)\Big((u_2-u_1)^2+(w_2-w_1)^2\Big)\right\}\Big]f_1f_2d\mathbf{c}_1d\mathbf{c}_2. \tag{A. 18}$$